How volcanic stratigraphy constrains headscarp collapse scenarios : the Samperre Cliff case study (Martinique Island, Lesser Antilles)

Marc Peruzzetto[1], Yoann Legendre[1], Aude Nachbaur[2], Thomas J.B. Dewez[1], Yannick Thiery[1], Clara Levy[1], and Benoit Vittecoq[2]

[1]BRGM, F-45060 Orléans, France
[2]BRGM Martinique, 97200 Fort-de-France, Martinique

Correspondence: Marc PERUZZETTO (m.peruzzetto@brgm.fr)

Abstract. Gravitational instabilities can be significant threats to populations and infrastructures. For hazard assessment, it is of prior importance to estimate the geometry and volume of potential unstable masses. This characterization can be particularly difficult in volcanic context due to the succession of deposition and erosion phases. Indeed, it results in complex layering geometries where the interfaces between geological layers may be neither parallel nor planar. Geometry characterization is all the more complex when unstable masses are located in steep and hardly accessible landscapes, which limits data acquisition. In this work, we show how remote observations can be used to estimate the surface envelope of an unstable mass on a volcanic cliff. We use ortho-photographs, aerial views and topographic surveys to (i) describe the different geological units of the cliff, (ii) *identify stable and unstable***characterize the stability of geological** units, (iii) infer the paleo-morphology of the site and (iv) estimate potential unstable volumes. We *use***investigate** the Samperre cliff in Martinique (Lesser Antilles, French West Indies) as a study site, where recurrent destabilizations since at least 1988 have produced debris flows that threaten populations and infrastructures. Our analysis suggests that the destabilizations occurring on the cliff may be associated to the re-opening of a paleo-valley filled by pyroclastic materials. We estimate that between 3.5×10^6 m^3 and 8.3×10^6 m^3 could still be mobilized by future destabilizations in the coming decades.

1 Introduction

Volcanoes alternate construction phases, when eruption materials widen and heighten the volcanic edifice, and destruction phases *leading to the progressive***contributing to the** dismantling of the edifice (Thouret, 1999) **and to its progressive widening (e.g. De Rita et al., 1997; Manville et al., 2009; Di Traglia et al., 2020)**. Such destruction phases occur sometimes very violently during caldera forming eruptions, e.g. during the Samalas 1257 CE eruption (Lavigne et al., 2013) or the Tambora 1815 CE eruption (Stothers, 1984). The erosion of volcanic edifices also results from gravitational insatiabilities because of the mere construction mechanism of volcanoes, by progressive accumulation of eruptive materials (Ramalho et al., 2013). **Volcanic structures are the result of alternating periods of deposition and erosion. Between these phases the materials are often subjected to strong alteration, especially in tropical and subtropical contexts. Thus, there can be strong disparities in the geotechnical and hydrogeological characteristics of the different successions of lithological layers or**

even within the same layer. These geometrical and internal disparities favour gravitational instabilities, especially when the morphology is favourable.*In volcanic context, gravitational instabilities are favoured or triggered by various factors (see Schaefer et al. (2019) for a review). They include***These predisposing factors can be accentuated (see Schaefer et al. (2019) for a review) by** steep slopes (e.g. on steep walled andesitic edifices, Voight, 2000), hydrothermal alteration (Revil et al., 2020; Heap et al., 2021), hydrothermal pressurization (Reid, 2004), rainfall (van Wyk de Vries et al., 2000) *and* **,**earthquakes (Coviello et al., 2021) **and eruptions (Siebert et al., 1987; Durand et al., 2018)**. *Eruptions favor gravitational instabilities (Siebert et al., 1987; Durand et al., 2018), but are not necessarily the main triggering factor (Cutler et al., 2022).* The scale of instabilities varies from a few m^3 (e.g. for rockfalls, Durand et al., 2018) to large debris avalanches up to several km^3 (sector or flank collapse, Blahůt et al., 2019).

Since the dramatic flank collapse of Mount St Helens in 1980 (Voight et al., 1983), massive debris avalanches (more than 10^7 m^3) have been widely studied (e.g. Siebert et al., 1987; Voight, 2000; Boudon et al., 2007). Siebert (1984) estimates a worldwide occurrence frequency of about 4 such events per century. *Site***, but site** specific occurrence frequencies are variable. For instance, the Soufrière de Guadeloupe volcano has produced at least 8 flank collapses in the past 9,150 years (Komorowski et al., 2005; Legendre, 2012). With one event per 1,100 yr on average, flank collapse events appear rather frequent on a geological time scale. However, from a human perspective this represents only one event in 45 generations.

In comparison, smaller mass wasting events (from 10^6 to 10^7 m^3) are more frequent. Landslide occurrence rate f is indeed related to landslide volume V through a power law $f \propto V^{-\beta}$, withβ a positive parameter. For instance, Brunetti et al. (2009) estimate $\beta = 1.3$ for a global dataset of landslides ranging from 10^{-4} to 10^{13} m^3 (including among others rockfalls, rock avalanches and debris avalanches). When considering landslides in volcanic context only, Brunetti et al. (2009) compute $\beta = 1.1$ (see their dataset R). Thus, although mass wasting events involving 10^6 to 10^7 m^3 affect smaller areas in comparison to larger volcanic flank collapse (>10^8 m^3), their higher occurrence rate may result in similar risk levels.

In volcanic context, events involving 10^6 to 10^7 m^3 span a wide variety of landslide type, including slow moving landslides (a few cm yr^{-1} to a few m yr^{-1}) as in the Salazie cirque in La Réunion island, France (Belle et al., 2014; Rault et al., 2022), partial dome collapse during eruptive episodes (Harnett et al., 2019), and very fast (several tens of m s^{-1}) rock or debris avalanches during or long after eruptive episodes (e.g. 2010 Mount Meager landslide in Canada, Guthrie et al., 2012; Moretti et al., 2015). In this study we focus on such rock and debris avalanches. They can be significant threats to populations and infrastructures *due to their velocity and the difficulty***as they can occur far from current eruptive centers, and thus in urbanized areas. Besides, it is difficult** to predict their occurrence. For instance, 2500 people were killed by the 1.6×10^6 m^3 Casita (Nicaragua) debris avalanche in 1998 during hurricane Mitch (van Wyk de Vries et al., 2000; Scott et al., 2005). **Another example is the Grand Sable rock avalanche (about 20×10^6 m^3) that killed 62 people in Réunion island in 1875 (Humbert et al., 1981; Rault et al., 2022).**

In order to assess the risks associated to debris and rock avalanches, their propagation and the associated impact on populated areas can be estimated through numerical modelling (e.g. McDougall, 2017; Peruzzetto et al., 2019) or empirical laws (e.g. Mitchell et al., 2019; Peruzzetto et al., 2020). However, a major difficulty in such studies is the characterization of the **geometry and volume of the** initial unstable mass, that is, the initial conditions of propagation simulations. **When the land-**

slide has already occurred, they are usually reconstructed using topographic surveys carried out before and after the event. For potential future landslide, the failure surface (or at least the surface separating stable and less stables units) must be inferred. Its extent can be deduced from field observations and/or records of surface displacements (e.g. with satellite monitoring, Schaefer et al., 2019; Hickey et al., 2020). Then, when the subsurface is homogeneous, the failure surface *enveloppe separating stable and less stable units* **can be estimated with relatively simple geometric considerations (Jaboyedoff et al., 2019, 2020).***The initial unstable mass is characterized by its volume and/or its geometry. Both can be determined from the surface envelope separating the stable and unstable materials, and corresponding to potential rupture surfaces. This envelope can be deduced from the extent of the landslide on the topography and relative simple geometric considerations, provided the subsurface is homogeneous (Jaboyedoff et al., 2019, 2020). The determination of the landslide extent is a problem by itself: it can be inferred, for instance, from field observations or records of surface displacements (e.g. with satellite monitoring, Schaefer et al., 2019; Hickey et al., 2020).* However, **as already said,** the sub-surface is often not homogeneous in volcanic environment*, because different volcanic materials were deposited during successive eruptions with erosion and weathering phases in between. To construct the surface envelope, i***I**t is thus necessary to identify the different geological units composing the unstable slope. This requires field work and/or geophysical surveys (Rosas-Carbajal et al., 2016, 2017). The nature and geometry of geological units can then be processed in a expert way to identify preferential rupture surfaces. Rupture surfaces can also be inferred from limit equilibrium analysis, provided geotechnical data is available (Apuani et al., 2005; Verrucci et al., 2019; Heap et al., 2021).

However, in many cases, researchers and/or practitioners can only rely on remote observations and/or topographic models to estimate the surface envelope of the unstable mass. This happens when field work is difficult or dangerous (e.g. in remote and steep areas), and when advanced remote sensing methods are not applicable (e.g. InSAR acquisition for displacement measurements does not yield conclusive results in densely vegetated areas). *Besides, in volcanic context, simple geometric considerations linking the rupture surface to the extent of the unstable mass may not be applicable either (Jaboyedoff et al., 2019, 2020): the volcanic formations below the surface are often not homogeneous and can display complex geometries.* In these conditions where relatively few data are available but stakes require a quantified hazard assessment, how can we estimate the surface envelope of an unstable mass, from which the unstable volume can be quantified?

In this work, we show how the combined use of historical ortho-photographs and aerial photographs, Digital Elevation Models (DEMs) and 3D point clouds can help estimate the surface envelope of an unstable mass. We *choose***investigate** the Samperre cliff in Martinique (Lesser Antilles, French West Indies) as a case study. Located on the western flank of the Montagne Pelée volcano, it has undergone several episodes of destabilizations since at least 1980 or even 1950 (Aubaud et al., 2013; Clouard et al., 2013). Although the resulting rock avalanches do not threaten directly populated areas, subsequent debris flows do propagate several kilometers downstream and impact populations, buildings and infrastructures. The quantification of potentially unstable volumes is thus important to assess the volume of the resulting loose debris reservoir that could feed debris flows.

The geological context of the study site is given in Section 2. In Section 3 we present the topographic surveys and ortho-photographs used in this work, along with the methods used to (i) characterize the geometry of geological units and (ii) compute

the volume of the unstable mass. Then, in Section 4, we describe the different geological layers forming the Samperre cliff and differentiate between stable and unstable layers **(given the current morphology of the cliff)**. This allows to infer the paleo-morphology of the site and identify *a paleo-valley* **the paleo-surface of a valley progressively filled by volcanic deposits**. We extrapolate the geometry of this *paleo-valley* **paleo-surface** to construct a stable basal surface above which materials *can* **could** be remobilized. The associated volume is computed and discussed in Section 5, along with the other results of our work.

2 Study site

A detailed review of Martinique island geological history can be found in Westercamp et al. (1989); Maury et al. (1991); Boudon et al. (2005); Germa et al. (2011); Boudon and Balcone-Boissard (2021). The Martinique island is part of the Lesser Antilles volcanic arc (Figure 1). The Samperre cliff is located in the northern part of the island, in the most recent volcanic formations and constituting since 550 kyrs the Montagne Pelée Volcanic Complex *(Boudon and Balcone-Boissard, 2021, Figure 1a and)* **(Figure 1b and Boudon and Balcone-Boissard, 2021)**.

The first **building** stage of Montagne Pelée Volcanic Complex is a succession of andesitic breccias, lava domes and lava flows dated between 550 and 127 kyrs by Germa et al. (2011). The end of the first stage is marked by the Prêcheur flank collapse (Prêcheur collapse structure in Figure 1, Le Friant et al., 2003; Boudon and Balcone-Boissard, 2021). This 25×10^9 m^3 collapse (Brunet et al., 2016) entailed a lithostatic decompression of the lava chamber feeding this primitive Montagne Pelée edifice (Germa et al., 2011). It may have triggered the formation of the Piton Marcel lava dome near the boundary of the horse-shoe shaped collapse structure (Figure 1*b***c**).

The Prêcheur flank collapse marks the the beginning of the second phase of the Montagne Pelée Volcanic Complex. Lava dome-forming eruptions and associated concentrated pyroclastic density currents were the dominant activity. The edifice that grew in the Prêcheur collapse scar was destroyed by another flank collapse about 36 kyrs ago (Rivière Sèche collapse, Solaro et al., 2020). During the third **building** stage of the Montagne Pelée Volcanic Complex, the first 10 kyrs years were characterized by abundant explosive activities with low-silica andesitic magma. Over the past 25 kyr, Boudon and Balcone-Boissard (2021) have recorded at least 55 magmatic eruptions, two third of which are dome forming eruptions, and the rest being plinian eruptions.

The volumes of flank collapses can be estimated from the on-land and submarine topography. However, before the new interpretation of Solaro et al. (2020), previous studies suggested the Prêcheur flank collapse 127 kyrs ago was constituted of two separate collapses, 127 kyrs and 32 kyrs ago (Le Friant et al., 2003; Germa et al., 2015; Brunet et al., 2016). Their volumes were estimated to 25×10^9 m^3 and 13×10^9 m^3 by Brunet et al. (2016). Smaller volumes were computed by Germa et al. (2015) using a geomorphological analysis: 14.7×10^9 m^3 and 8.8×10^9 m^3. Thus, the total volume for the Prêcheur collapse can be estimated between 27.5×10^9 m^3 and 38×10^9 m^3. However, these volumes were likely destabilized by successive smaller debris avalanches less than 5×10^9 m^3, as suggested by numerical simulations (Brunet et al., 2017). Such volumes are coherent with the volume estimated for the Rivière Sèche flank collapse, between 2×10^9 m^3 (Brunet et al., 2016) and 3.5×10^9 m^3

(Germa et al., 2015). Even so, the magnitude of such events is about 100 to 1,000 times larger than that of the rock avalanches we focus on (less than 10^7 m^3).

*Such r*Rock avalanches **involving up to 10^7 m^3** occur in the Prêcheur river catchment that drains part of the western flank of Montagne Pelée. The Prêcheur river's major affluent is the Samperre river*. The Samperre river* **that** skirts Piton Marcel to the south and has its source at the toe of Samperre cliff. This cliff is very recent, as it was formed between 1951 CE (when only smooth slopes are visible on ortho-photographs) and 1980 CE (first monitored collapse) by successive retrogressive failures (Figure 2). Five major destabilization sequences occurred in 1980, 1997-1998, 2009-2010 and 2018 (Aubaud et al., 2013; Nachbaur et al., 2019), but another unconfirmed collapse episode may have happened in the 1950s (Aubaud et al., 2013). Thus, the cliff rim has retreated by 250 m between 1988 and 2018 along a West-South-West / East-North-East direction (azimuth N062°*E* **measured clockwise as all azimuth direction in this work**, white line in Figure 2a), resulting in a 300 m high steep ($> 60°$) to sub-vertical wall. Clouard et al. (2013) estimated that a volume of about 2.1×10^6 m^3 collapsed between March and May 2010. Between May 2010 and August 2018, the cliff lost about 4.9×10^6 m^3, with a major collapse sequence between January and August 2018 (Quefféléan, 2018; Nachbaur et al., 2019; Peruzzetto, 2021b; Peruzzetto et al., 2022). These destabilizations are often (if not systematically) associated with the remobilization of deposits **by water** and the generation of debris and hyper-concentrated flows. For instance in June 2010, a major debris flow inundated part the Prêcheur village at the river mouth and severely damaged the bridge crossing the river (Aubaud et al., 2013; Peruzzetto et al., 2022). A new and higher bridge has since been constructed, but major lahars could still destroy it. As a result, about 420 people would be isolated from the rest of the island (INSEE, 2015). For *a* local risk management *perspective*, it is thus important to assess the volumes of future rock avalanches from the Samperre cliff in order to estimate the magnitude of the associated debris flows and to quantify the **resulting** risk**s** *for exposed population*.

3 Material and methods

Our objective is to *assess the surface envelope of potentially unstable volumes from the Samperre cliff***quantify the volume that could still collapse from the Samperre cliff in the coming decades**. To that end, we need to **analyze** the geology of the cliff and infer the geometry of geological units. As field work is too dangerous and because *we have* no geophysical data **are available**, we must *only* rely on remote observations and topographic surveys **only**.

3.1 Data

Over the past decades, and in particular since the first documented collapse sequence in 1980, numerous oblique aerial pictures taken during helicopter surveillance flights have documented the evolution of the cliff. We use them **along** with georeferenced ortho-photographs. The oldest available ortho-photographs date back to 1951 (IGN, 2021a, b). *The next one were acquired in 1988 and then more regularly until 2018***6 other ortho-photographs are then available for the 1988 - 2018 period**. The date and details of acquisitions are given in Table 1. The comparison between successive photographs document the plan-view

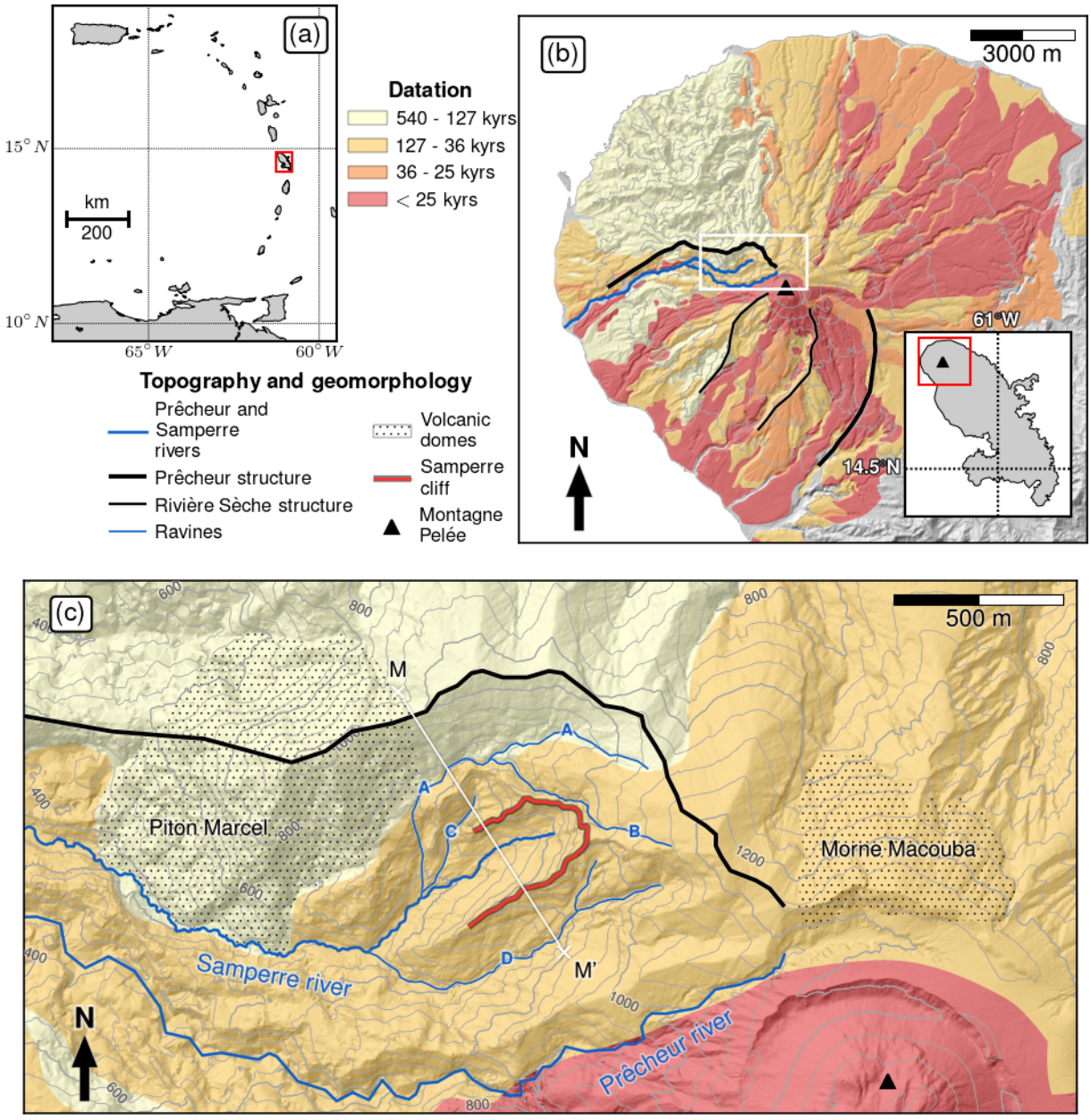

Figure 1. Map of the study site. **(a) Map of the Lesser Antilles. Martinique island is located in the red rectangle.** (*a***b**) Geological map of Montage Pelée volcano, adapted from Westercamp et al. (1989) using the interpretation of Boudon and Balcone-Boissard (2021). The main phases of volcanic activity are: first **building** stage / Primitive Montagne Pelée (550-127 kyrs), second **building** stage / Intermediate Montagne Pelée (126-36 kyrs) and third **building** stage / Recent Montagne Pelée (35-26 kyrs, and 25 kyrs-present). Older formations and alluvial deposits are not mapped. The insert is Martinique island. The red rectangle in insert gives the extent of *a***b**. The white rectangle in *a***b** gives the extent of *b***c**. *b***(c)** Close-up on the North-West flank of Montagne Pelée, with the Samperre Cliff, Piton Marcel, Morne Macouba, the Prêcheur and Samperre rivers, and main ravines. Ravines are are referred to with letters A, B, C and D in the text. The destabilization structures are reproduced from Boudon and Balcone-Boissard (2021).

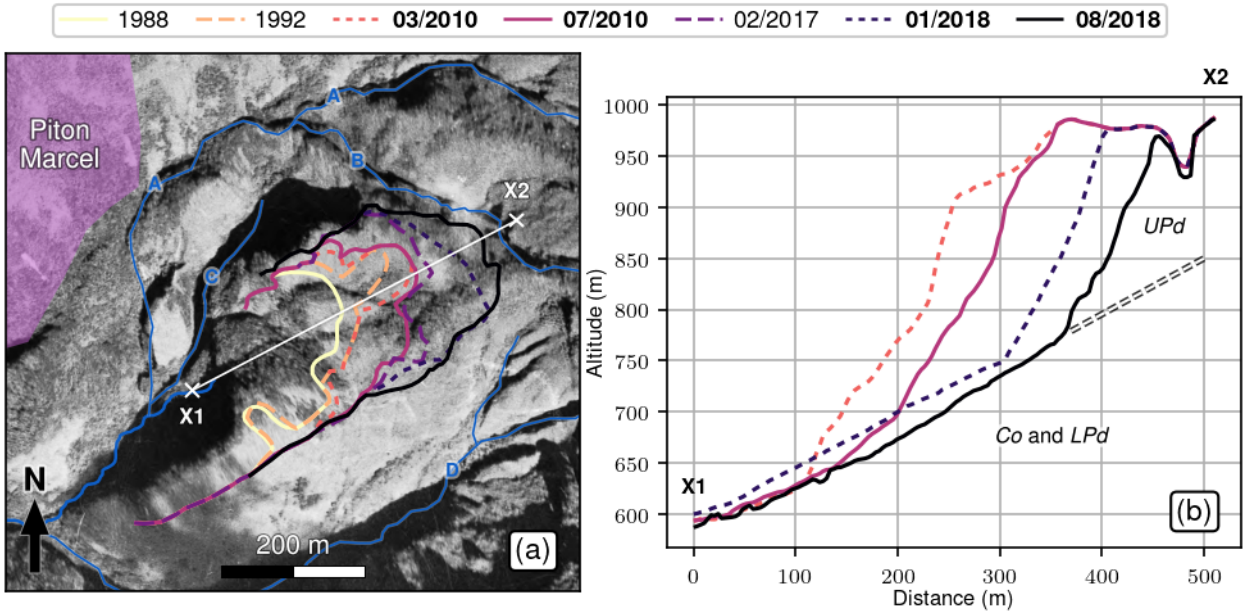

Figure 2. Evolution of the Samperre Cliff between 1951 and 2018. (a) 1951 ortho-photograph of the Samperre cliff. The successive cliff rims observed on ortho-photographs and DEMs between 1988 and 2018 are given by plain and dashed lines. The Samperre river (thick blue line), ravines (thin blue lines) and the Piton Marcel (purple patch) are given as in Figure 1. (b) Successive cross-sections of the cliff (03/2010, 07/2010, 01/2018, 08/2018, in bold in the legend). The inferred contact between the stable unit *UPd*, and unstable units *Co* and *LPd* is given by the white dashed line. The extent of the cross-section is reported in (a) by the segment [X1, X2].

recession of the cliff and its geology **(Figure 2)**. We analyze in details the 08/2018 ortho-photograph to identify visually the different geological units composing the Samperre cliff from color or texture variations.

Several DEMs and 3D point clouds are also available, derived from LiDAR or photogrammetric acquisitions between March 2010 and August 2018 (see Table 1). They are used to characterize the geometry of identified geological units by means of the CloudCompare software (CloudCompare, 2020). We characterize (i) deposition horizons identified by sharp color contrasts, (ii) interfaces between units inferred from slope breaks and (iii) the surface of outcrops.

3.2 Geometric characterization of geological layers

We do not use the 08/2018 ortho-photograph to characterize deposition horizons because the Samperre cliff displays steep and even over-hanging topographic features. Instead, we work directly on textured 3-D point clouds that allow a better characterization of geometric features (e.g. Pavlis and Mason, 2017; Buckley et al., 2019). The horizons are thus identified on the 07/2010 photogrammetric 3D point cloud **(Figure 3)**. This point cloud has the best resolution compared to other point clouds of the area (on average, 32 pts/m^2 on the cliff). Horizons are picked in CloudCompare (CloudCompare, 2020) with the *Compass* plug-in (Thiele et al., 2017). This plug-in automatically interpolates paths between manually picked points, with a least-cost-path

Table 1. Ortho-photographs and topographic surveys.

	Date	Resolution / Précision	Use	Source	Comment
Ortho-photograph	1951, 1988, 1992 03/2010, 02/2017	0.5 m/pixel	- Cliff rim position	BD ORTHO®, BD ORTHO®Historique (IGN, 2021a, b)	n.a.
	07/2010	0.2 m/pixel	- Cliff rim position - Geological units	Ortho Hélimap/DEAL 972	n.a.
	08/2018	0.05 m/pixel		Ortho Hélimap/DEAL 972	n.a.
DEM derived from LiDAR	03/2010	1 m/pixel	- Cliff rim position - Unstable volume quantification	IGN Litto3D®	Acquisition over the whole Martinique island
	08/2018		- Cliff rim position - Basal surface for unstable volume quantification	Hélimap company	Acquisition limited to the Samperre cliff, Samperre river and Prêcheur river
Photogrammetric model	07/2010	32.3 pts/m^2	- Cliff rim position - Basal surface for unstable volume quantification - Sedimentary interfaces	Pictures: Hélimap company 3D model: this study, with Agisoft Metashape	n.a.
	01/2018	22.5 pts/m^2	-Cliff rim position	Pictures: Carige company 3D model: this study, with Agisoft Metashape	n.a.

solver, provided a cost function. As deposition horizons are identified by color change, we choose a cost function that depends on RGB (Red Green Blue) color gradient: the resulting path is chosen such that it follows strong RGB gradients. We pick horizons that are first identified by visual inspection of the point cloud **(Figure 3a)**. *Compass* is also used to pick interfaces marked by a slope break: in this case, the cost function depends on the point cloud local curvature.

To assess the dip and dip direction of the deposition horizons and interfaces, we sample points along the picked polylines (10 pts/m). The resulting point cloud is then fitted by a plane. The quality of the fit is given by the Root Mean Square (RMS) of the distances from the points to the best-fit plane. Following Fernández (2005), we also compute two indicators, M and K (see Appendix A for computation details). Fernández (2005) suggest that $M > 4$ indicates a good fit between the plane and the point cloud, and that $K < 0.8$ indicates a correct estimation of the plane orientation. Sampling bias results in an estimation uncertainty on dip and dip direction. We quantify this uncertainty by computing the 100-times bootstrapped standard deviation of dip and dip direction (see Appendix A for details).

The same methodology is used to estimate the dip and dip orientation of outcrop surfaces extracted from point clouds.

3.3 Unstable volume quantification

The identification of the different geological units, the characterization of their geometry, and their evolution since 1950 *evidences***documents** the progressive unearthing of interfaces limiting the basal and lateral surface of *the* successive destabilization*s* **epsiodes**. Thus, we can differentiate between geological units affected by destabilisations and geological units that *are***have remained** stable*s*. These observations are used to reconstruct the paleo-morphology of the site and infer a basal stable surface above which materials are unstable.

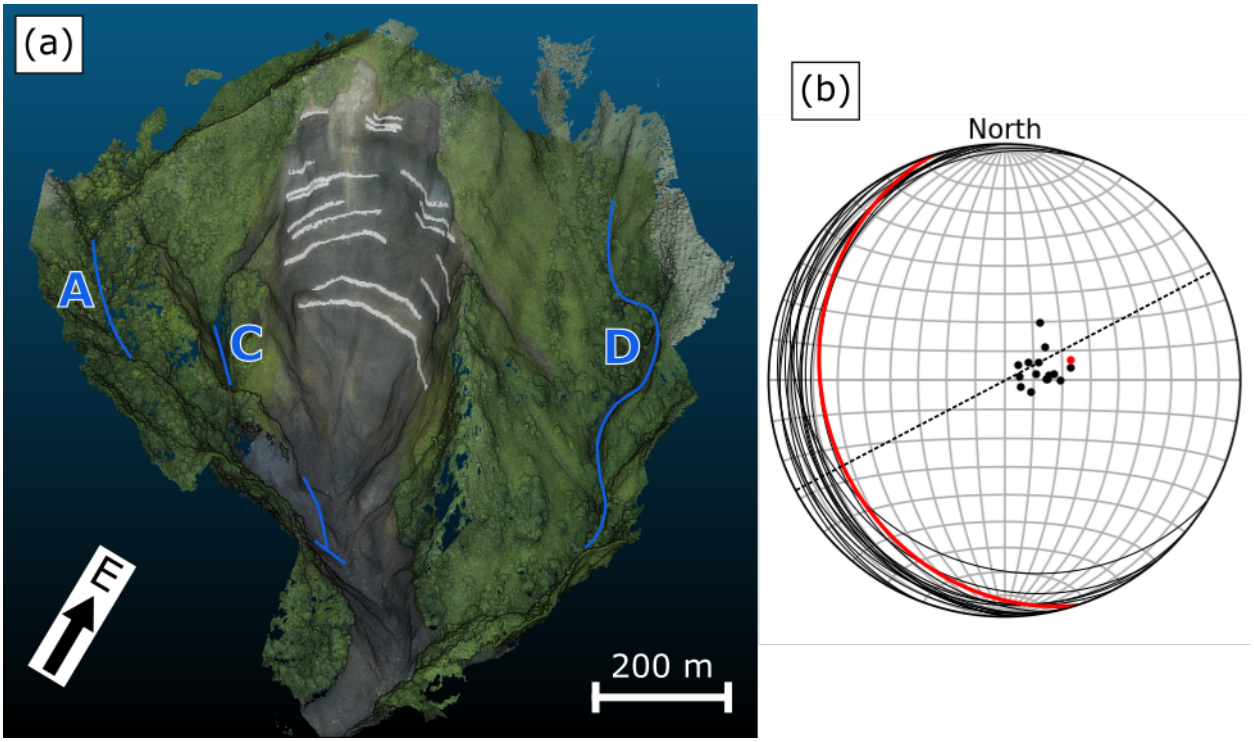

Figure 3. Deposition horizons orientation. (a) July 2010 photogrammetric 3D model, with deposition horizons (white lines). Ravines are highlighted by blue lines with their name, as in Figure 1. (b) Wolff stereonet projection of deposition horizons (black lines), with corresponding poles (black dots). The contact *S0* between LPd and UPd is also given in red. The black dashed line gives the cliff retreat direction (azimuth N062°*E*, white line in Figure 2)

This basal surface is composed of (i) outcrop surfaces of geological units considered stable*s* (approximated by planes, as described in the previous section) and (ii) planes fitted manually in CloudCompare to topographic features that have remain**ed** stable since 1951. The potentially unstable volume is then defined as the rock mass contained between this basal surface, and the topography (08/2018 DEM for the cliff, 03/2010 DEM elsewhere). Given the 1 m **horizontal** accuracy of the DEM, we consider only height difference superior to 1 m, in an area above the contact between the stable and unstable geological units.

The computed rock mass volume is dependant upon the different modelled planar units. To estimate volume variations caused by sampling bias, we randomly resample 100 times the outcrop surfaces of stable geological units and derive the associated best-fit planes and resulting basal surface. Then, we compute the bootstrapped standard deviation of the potential unstable volume.

4 Results

In this section (i) we describe geological units composing the Samperre cliff, (ii) we *identify which units are stable are which units are unstable***characterize the relative stability of each unit**, (iii) we reconstruct the paleo-morphology of the site, and (iv) we use these results to reconstruct the **possible** surface envelope of *the* **an** unstable mass and compute the corresponding volume.

4.1 Geological description of the cliff

The different geological units composing the Samperre cliff (Figure 4) have been progressively exposed by successive destabilization episodes. In the following we describe the successive layers from top to bottom.

The top most layer of the cliff is composed by brown to light brown, probably weathered materials (unit *Pu*, yellow patch in Figure 4c). It was exposed in 2010 as a 20 to 30 meter thick layer (Figure 5a), as mentioned by Mathon and Barras (2010) and Clouard et al. (2013). The 2018 destabilizations removed most of this geological unit. By March 2018, the corresponding layer at the cliff head was only about 10 meter**s** thick (Figures 5b and 5c).

Below unit *Pu*, a massive, light gray to light brown, 50 m thick layer was exposed in 2018 to the East and South of the cliff (unit *La*, *blue***orange** patch in Figure 4c). This layer displays clear vertical prismatic patterns **(Figures 5b and 5c)**. We associate these patterns to *an andesitic lava flow (Figures 5b and 5c)***columnar jointing of tuffs (Lim et al., 2015; Hamada and Toramaru, 2020) rather than to a lava flow, because no recent lava flow has been identified in this sector in previous studies (Boudon and Balcone-Boissard, 2021)**.

Most of the cliff below **units *Pu* and *La*** is formed by a 100 to 200 m succession of *pyroclastic deposits***greyish materials** (unit *UPd*, *purple***pink** patch in Figure 4c). *They include several meters wide blocks.* The interface between successive deposits can be clearly identified by color changes, from light to dark gray (Figure 3a). **The deposits show significant variability in thickness and grain size distribution, with blocks several meters wide. We interpret unit *Upd* as pyroclastic deposits.** On the 07/2010 photogrammetric model, we approximate *these interfaces***the deposition horizons** by planes (Figure 3b), with mean dip 16° and dip direction N254°*E* (see Table A1). This is, to within 15°, the opposite direction of cliff retreat since 1950 (N062°*E*, black dashed line in Figure 3b).

The bottom part of the cliff is composed, in its North-West side, by a characteristic ocher unit (unit *Co* in Figure 4c**, dark blue patch**). Unit *Co* was initially unearthed in July 2010 (Figure 5a, surface *S1* in 4). Following the destabilizations of 2018, the initial outcrop extended North-Eastward (Figures 5c and 5d, surface *S2* in Figure 4). The outcrop surfaces *S1* and *S2* have, respectively, dip angle**s** 47° and 42°, and dip direction**s** N308°*E* and N252°*E*. Both surfaces do not correspond to any known tectonic fault. The transition between units *Co* and *UPd* is marked by a clear slope break (see Figure 4b and Figure 4c), and water seepages **(Figure 5c and 5d)**. Another ocher outcrop can be observed on the western side of ravine A, at the bottom of Piton Marcel *(black patch in Figure 4c)*. Because unit *Co* has a distinctive ocher color, seems more consolidated and impermeable, we interpret it as old hydrothermalized volcanic materials (e.g. Salaün et al., 2011). As the northern extremity of the Prêcheur collapse scar is located only a few hundred of meters away from unit *Co*, we make the hypothesis that the surface

of unit *Co* is associated to the Prêcheur flank collapse. It could either be the collapse scar itself, or the surface of a mega-block that slid and stopped in the vicinity of the source area (Figure 6a). In this perspective, unit *Co* corresponds to eruptive materials emplaced during the first **building** stage of Montagne Pelée Volcanic Complex.

On the opposite side of the cliff, to the South-East, unit *UPd* lies on top of another succession of **light gray** *pyroclastic* desposits, **that we interpret as pyroclastic deposits,** *light gray, more indurated* with no evidence of destabilizations or erosion since 2010. This unit, that we call the lower pyroclastic unit *LPd* (*orange***mauve** patch in Figure 4c), may have been already visible in 2010 in the South-East part of the cliff, but was more obviously visible after the 2018 destabilizations (Figure 5c and 5d). The visible outcrop of *LPd* (surface S3 in Figure 4) is roughly planar, with dip angle 47° and dip direction N308°*E*, which does not correspond to any known tectonic fault. **No deposition horizon could be clearly identified.** As for unit *Co*, the transition between *UPd* and *LPd* units is marked by a clear slope break (see Figure 4b and Figure 4c, black dashed line), accompanied by several water seepages. Another clear slope break can be observed on the other side of the cliff in the adjacent valley (ravine D). If we consider the areas at the junction between units *LPd* and *UPd* (i.e., black dashed lines in Figure 4b and Figure 4c), both slope breaks are roughly coplanar, and the associated plane *S0* has dip angle 24° and dip direction N252°*E*. This is consistent with horizons measured in unit *UPd* (compare red and black points in Figure 3).

Absolute dating is difficult without rock samples, as the Samperre cliff area is unsafe to wander through. Following our assumption that unit *Co* is associated to **the** first **building** stage of Montagne Pelée Volcanic Complex phase, it may be at least 127 kyrs old. Pyroclastic deposits within the collapse scar (units *LPd*) are more recent and could have been emplaced in between the Prêcheur flank collapse (127 kyrs) and the Rivière Sèche collaps (36 kyrs), as suggested by the geological map of Westercamp et al. (1989) and the interpretation of Boudon and Balcone-Boissard (2021). The upper pyrocalstic *despoits***deposits** unit*s* *UPd* would then correspond to the eruptive phase characterized *by dome-forming and plinian eruptions (starting 25 kyrs ago, Boudon and Balcone-Boissard, 2021)***by scoriaceous, low silica, andesitic products and associated to pyroclastic density currents (36-25 kyrs), and/or to the subsequent eruptive phase (25 kyrs - present) where dome-forming and plinian eruptions predominated (Boudon and Balcone-Boissard, 2021)**. *The origin of the lava flow unit* La *is uncertain, but could be associated with the formation of the neighboring Morne Macouba 12 kyrs ago (Germa et al., 2011)***The tuff unit *La* cannot be dated but was probably emplaced by the fallout of one of the 17 plinian to sub-plinian eruptions reported by Boudon and Balcone-Boissard (2021) between 25 kyrs and present time**. *Following Mathon and Barras (2010) and Clouard et al. (2013), we***Mathon and Barras (2010) and Clouard et al. (2013)** interpret unit *Pu* as pumices *emplaced by the***of the most recent** plinian eruption**,** P1**,** that occurred *between 1289 and 1398 CE (Boudon et al., 2005)* **in 1348 ±50 CE (Boudon and Balcone-Boissard, 2021)**. **This date is coherent with that of Nachbaur et al. (2019) who dated pumice deposits on the edge of the Prêcheur river ravine, about 1.5 km to the West, at 1285 ±25 CE. However, it is possible that the unit *Pu* also contains desposits of previous plinian eruptions, and in particular P3 (113 ±85 CE). This powerful eruption (1 km^3 of magma DRE) affected the whole flanks of Mount Pelée, and to the West of the summit, the associated deposits often lie below P1 deposits (Carazzo et al., 2012, 2020).**

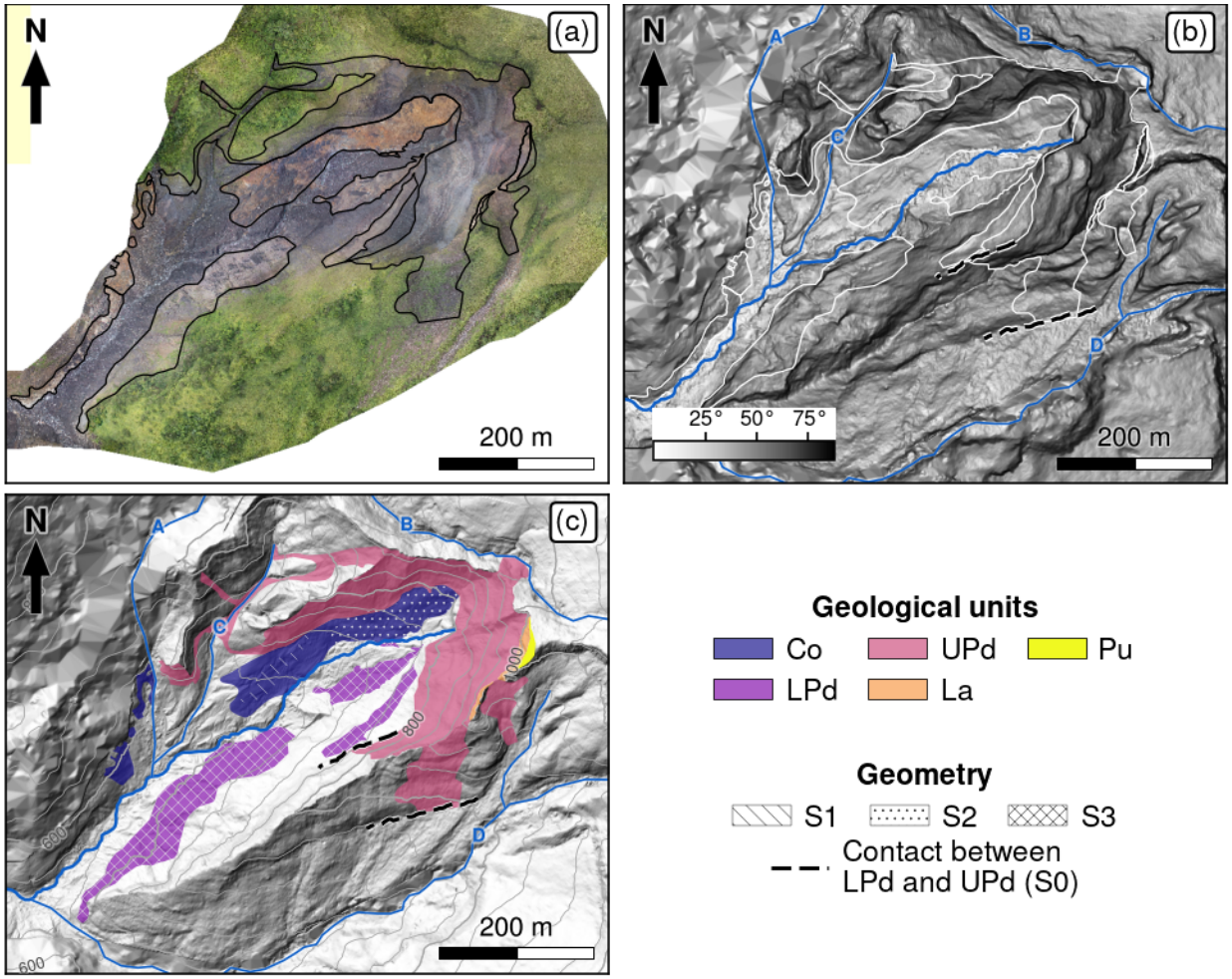

Figure 4. Geological interpretation of the Samperre cliff. (a) 08/2018 orthophotograph (Hélimap/DEAL 972), with contours of identified geological units. (b) Slopes of the 08/2018 DEM, completed with 07/2010 DEM , with contours of identified geological units. (c) 08/2018 DEM, completed with 07/2010 DEM. Colored patches correspond to geological units: *Co*, *LPd*, *UPd*, *La*, *Pu* (see main text for details). Hatched areas identify some of the surfaces used to construct a potential unstable volume (see Section 4.4). The contact between *LPd* and *UPd* units, inferred from slope breaks, is given in (b) and (c) by the black dashed lines. Ravines and rivers are also displayed, as in Figure 1.

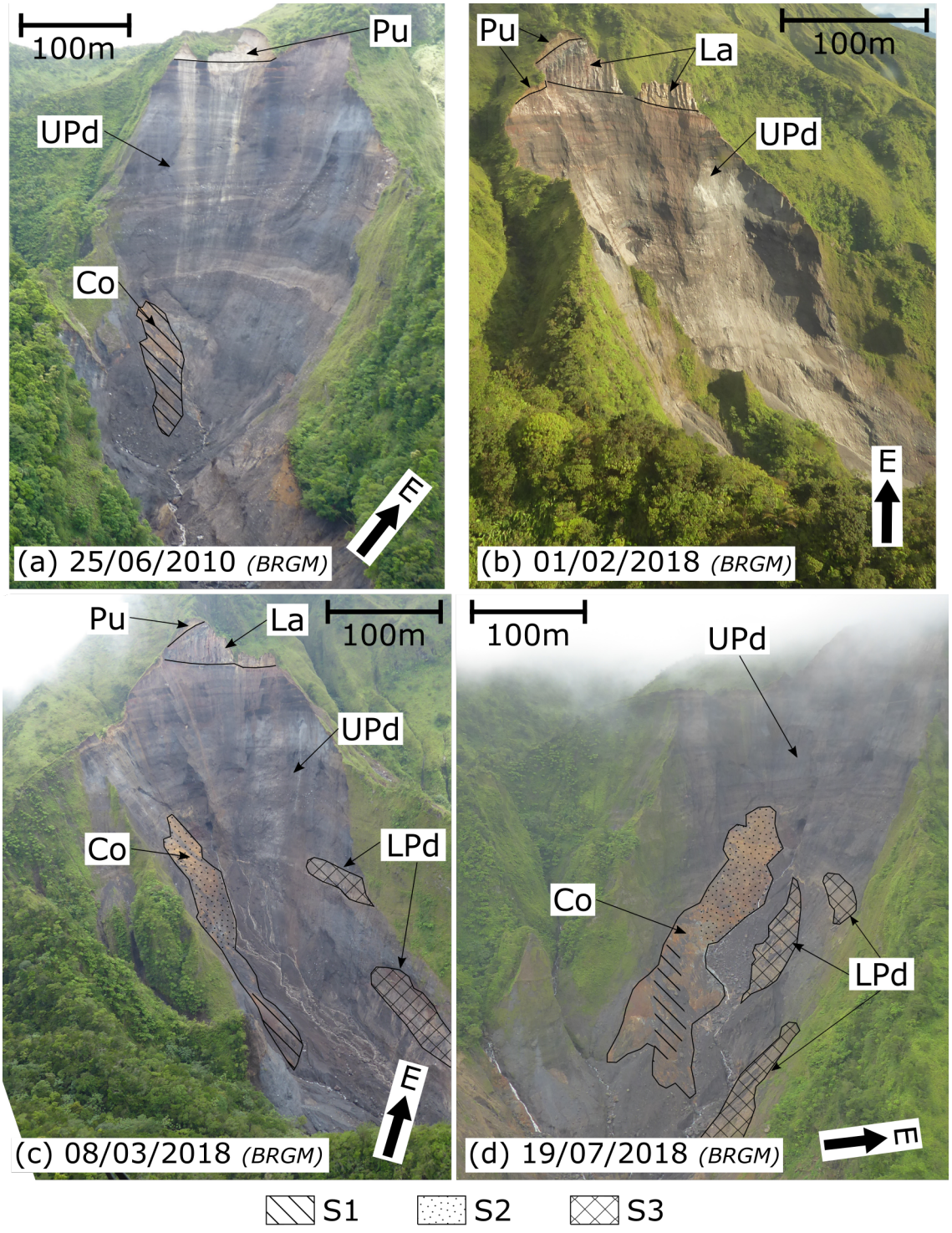

Figure 5. Aerial photographs of the Samperre cliff on (a) Jun. 25, 2010, (b) Jan. 2, 2018, (c) Mar. 8, 2018 and (d) Jul. 2, 2018. East direction is given by the arrow, the scale is given for the cliff rim. Outcrops of visible geological units are highlighted. **Raw pictures (along additional pictures) are given in Supplementary Materials.**

4.2 *Identification of stable and unstable*Relative stability of geological units

From successive ortho-photographs and topographic surveys (Figure 2), as well as aerial photographs (e.g. Figure 5a and 5b), it is clear that the upper geological units *Pu*, *La* and *UPd* are involved in the main destabilization*s* episodes. Thus, we conclude they are unstable. Following NGU (2012), the presence of water seapge at the base of unit *UPd* also favors its instability.

Units *Co* and *LPd* were previously *re*covered by unit *UPd*. Successive destabilizations have increased the surface of the outcrops. These outcrops do not display any clear collapse scar. They have remained relatively intact since they were exposed (e.g. compare outcrop of unit *Co* in Figures 5a and 5c). This suggests units *Co* and *LPd* are more resistant than unit *UPd*. This stability is further confirmed by water resurgences at the base of unit *UPd*, which indicates that the stability of units *Co* and *LPd* is less affected by increased pore pressures.

Thus, we make the hypothesis that units *Co* and *LPd* are **more** stable **than unit *UPd*, given the current morphology of the cliff**. From this assumption we deduce that the outcrop surfaces *S1* and *S2 (respectively* S3*)* correspond to the formerly hidden interface between units *Co (respectively* LPd*) and unit* Upd**and *UPd* (see Figures 6 and 7). Similarly, we deduce that the outcrop surface *S3* corresponds to the formerly hidden interface between units *LPd* and *UPd*.**

4.3 Paleo-morphology

From the geological and geometric observations described above we propose a scenario of the evolution of the catchment geomorphology, with successive construction and dismantling phases **(Figure 6)**.

Following the interpretation of Solaro et al. (2020), the Prêcheur flank collapse that occurred 127 kyrs ago is the oldest event that can be related to the current morphology of the Samperre cliff. This major dismantling event was followed by a construction phase*. The***, when the** accommodation space left by the collapse was progressively filled with new pyroclastic deposits (unit *LPd*, Figure 6a). Its surface may be given by the current interface between units *LPd* and *UPd* (surface *S0*).

A new dismantling phase then started **(Figure 6b)**. It may have been initiated by the Rivière Sèche flank collapse 36 kyrs ago: this collapse did not affect the Samperre cliff area but the resulting scar concentrated newly emitted volcanic materials. Thus, unit *LPd* was progressively eroded. We suggest erosion was mainly caused by preferential flow path along the Prêcheur collapse structure, and thus along unit *Co*. It led to the formation of a valley in a West-South-West/East-North-East direction (N062°*E*, Figure 6b). The North-West flank of the paleo-valley is given by surfaces *S1* and *S2* of unit *Co*, and the South-East flank by surface *S3* of unit *LPd*.

The emplacement of pyroclastic deposits from unit *UPd* corresponds to a new construction phase, when pyroclastic materials started filling the paleo-valley (Figure 6c). *Following Boudon and Balcone-Boissard (2021), this phase possibly started 25 kyrs ago.* Because deposition was geometrically constrained by the valley, successive deposition horizons from unit *UPd* have dip directions similar to that of the paleo-valley. **The beginning time of the filling of the paleo-valley is difficult to constrain without further dating data. Considering the previous dismantling phase started after the Rivière Sèche flank collapse 36 kyrs ago (see above), the filling of the paleo-valley is also posterior to that event. It may have ended when Montagne Pelée's eruption style changed 25 kyrs ago (Boudon and Balcone-Boissard, 2021).**

Then, a new, still ongoing, erosion phase started. As a result of permeability contrast between basal units *Co* and *LPd*, and upper unit *UPd*, underground water flowed preferentially at the interface between these units, that is, along the paleo-valley surface (as evidenced, today, by water seepages). It resulted in the progressive drainage of the paleo-valley by weakening the base of unit *UPd*, and thus favoring destabilizations. This process eventually led to the formation of the Samperre cliff (Figure 6d). It progressively retreated in the same direction as the paleo-valley. However, the erosion phase certainly started long before the known historical destabilizations, possibly as soon as the North-West flank of Montagne Pelée was no longer fed by eruptive materials.

As of 2022, *it***this erosion phase** is still an ongoing process. Thus, we suggest that the volumes that could be involved in future rock avalanches are constrained by the volume of materials filling the paleo-valley. To quantify this volume, we reconstruct the surface of the paleo-valley that we believe is **more** stable.

4.4 Assessment of unstable volume

The geometry of the paleo-valley is reconstructed by extrapolating outcropping surfaces of stable units and surfaces fitted to stable topographic features (see Section 3.3 for methodological details). These surfaces are displayed in Figure 7a, and their characteristics are given in Table 2.

The North-West (respectively South-East) side of the paelo-valley,is constrained by the surfaces *S1* and *S2* (respectively *S3*) of unit *Co* (respectively unit *LPd*). We also fit manually a planar surface *S4* to the North-West wall of ravine B, in the continuation of which we identified another outcrop of unit *Co* (see Figure 4c). Similarly, we fit a planar surface *S5* following the southern ridge of Samperre cliff, that has remained stable since at least 1988. Finally, we assume that the bottom of the paleo valley matches the current bed of the Samperre river (surface *S6*).

The resulting basal surface envelope is represented in Figure 7b. The height difference between the basal surface and the 2018 topography is displayed Figure 8. The corresponding volume is about 8.3×10^6 m^6. The uncertainty associated with least square plane fitting (but not to manual plane fitting) amounts to less than 1% of the estimated volume, and is thus negligible (see Table 3).

5 Discussion

5.1 Stability of unit *Co* and *Lpd*

We inferred from visual observations over more than a decade that units *Co* and *LPd* are more stable than unit *UPd*. In order to further investigate this hypothesis, we would need to characterize the geotechnical properties of these units. Geotechnical properties can be measured with in-situ tests (e.g. penetration tests) or with laboratory analysis of rock samples (e.g. tri-axial tests). However, both methods require field work that would be very dangerous near the Samperre cliff for safety reasons. **Samples could also be collected on outcrops of the same geological units located in more accessible areas. For the *UPd* unit, these outcrops could be identified by comparing their mineralogy, and age if possible, to that of lahars deposits in**

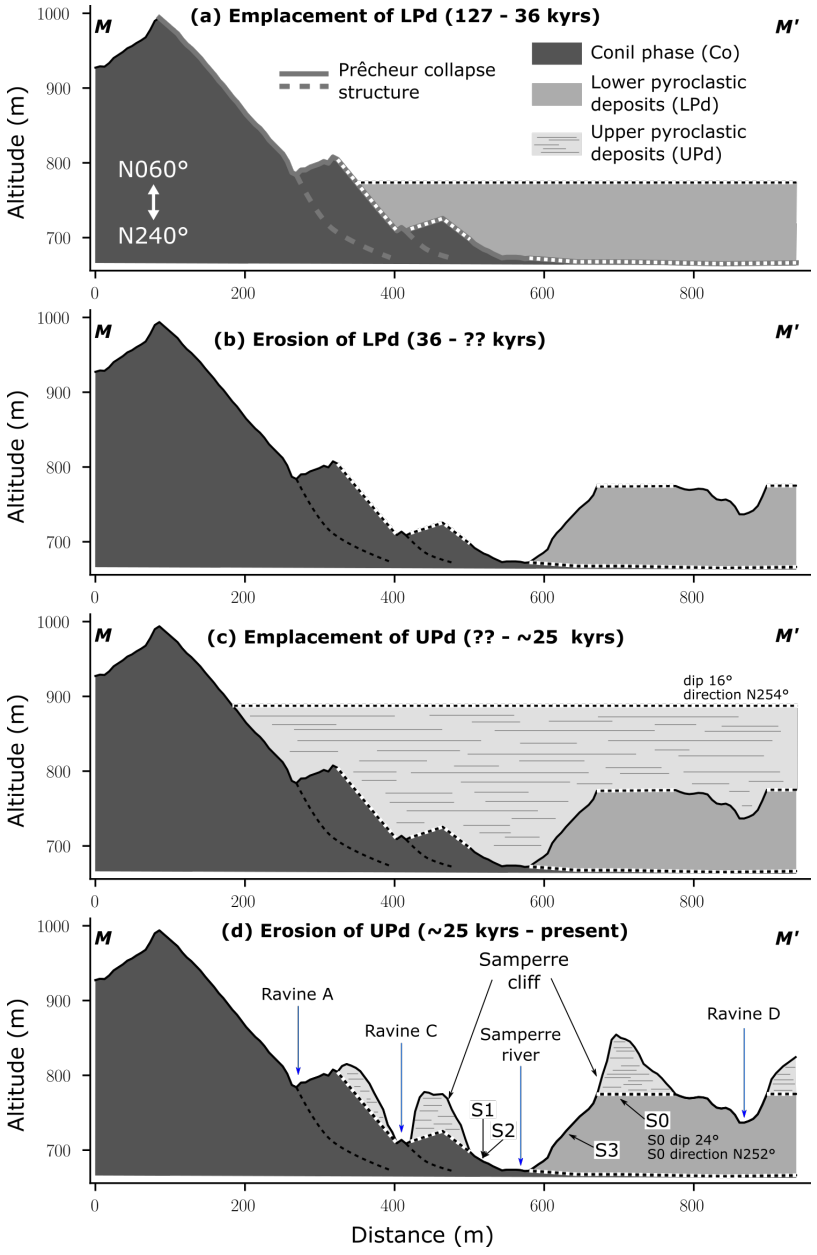

Figure 6. Conceptual view of the evolution of the paleo-morphology of the Samperre cliff, along a North-West (left) / South-East (right) cross-section (*MM'* in Figure 1b). **The figure is facing the North-East direction (N60°).** (a) Emplacement of unit *LPd* within the Prêcheur collapse scar. **The horizontal lines display deposition horizons, whose dip and dip direction are indicated).** (b) Erosion of unit *LPd*, resulting in a paleo-valley at the location of the actual Samperre cliff. (c) Emplacement of unit *UPd*. (d) Erosion of unit *UPd*, resulting in the formation of the Samperre cliff and adjacent ravines. Black plain line correspond to the topography given by the 08/2018 DEM. White dashed line are interpretations of old topographies and contact between geological units. See Figure 1c for the position of ravines.

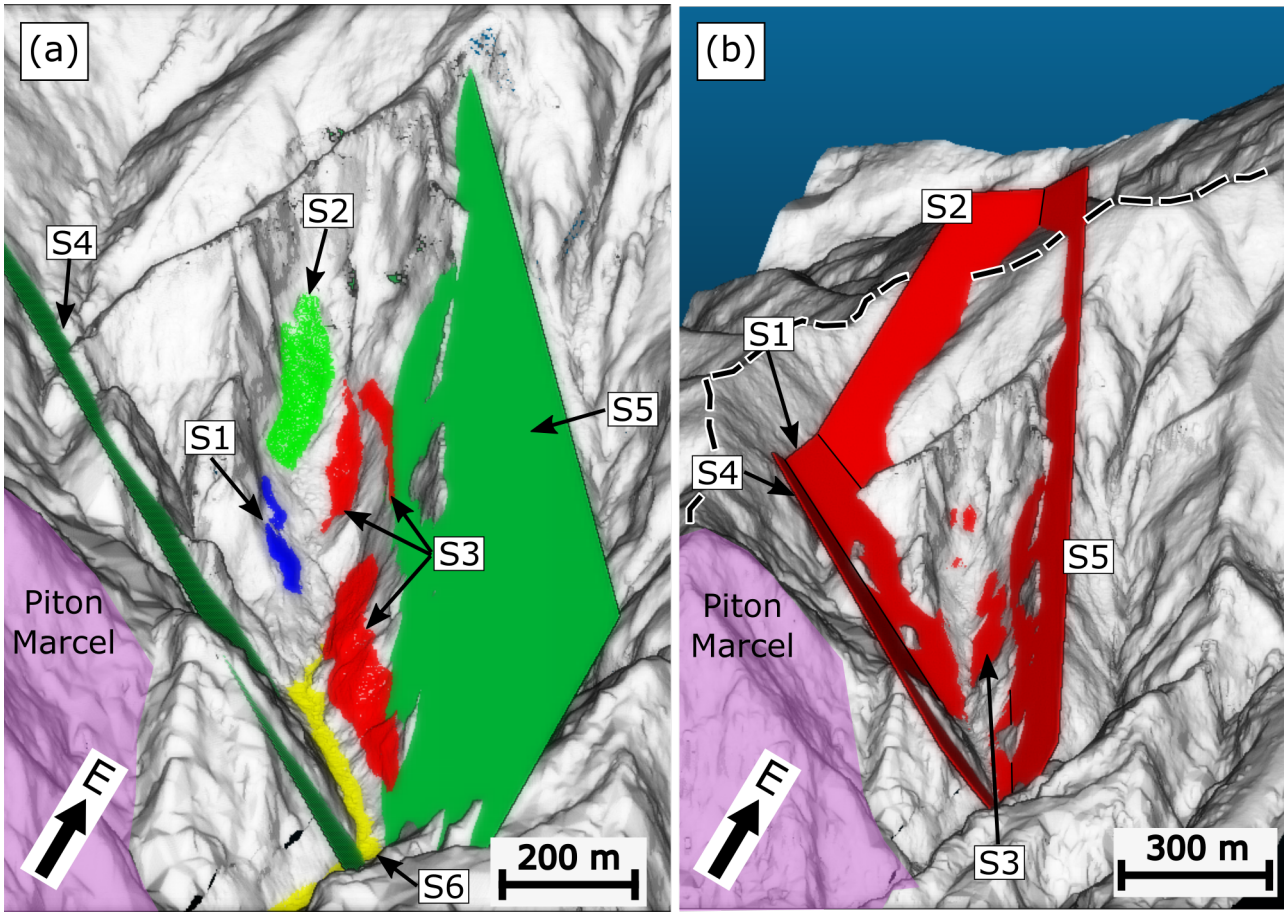

Figure 7. Construction of potential basal surface for unstable volume quantification. (a) Surfaces used to define the basal surface. S1 to S4 are point clouds extracted from DEMs, S5 and S6 are planes manually fitted to topographic trends (see Table 2). (b) Basal surface (red planes), constructed by extending and combining planes fitted to S1, S2, S3 and S4, and planes S5 and S6. The Piton Marcel is highlighted by the purple patch. The black dashed line is the Prêcheur destabilization structure.

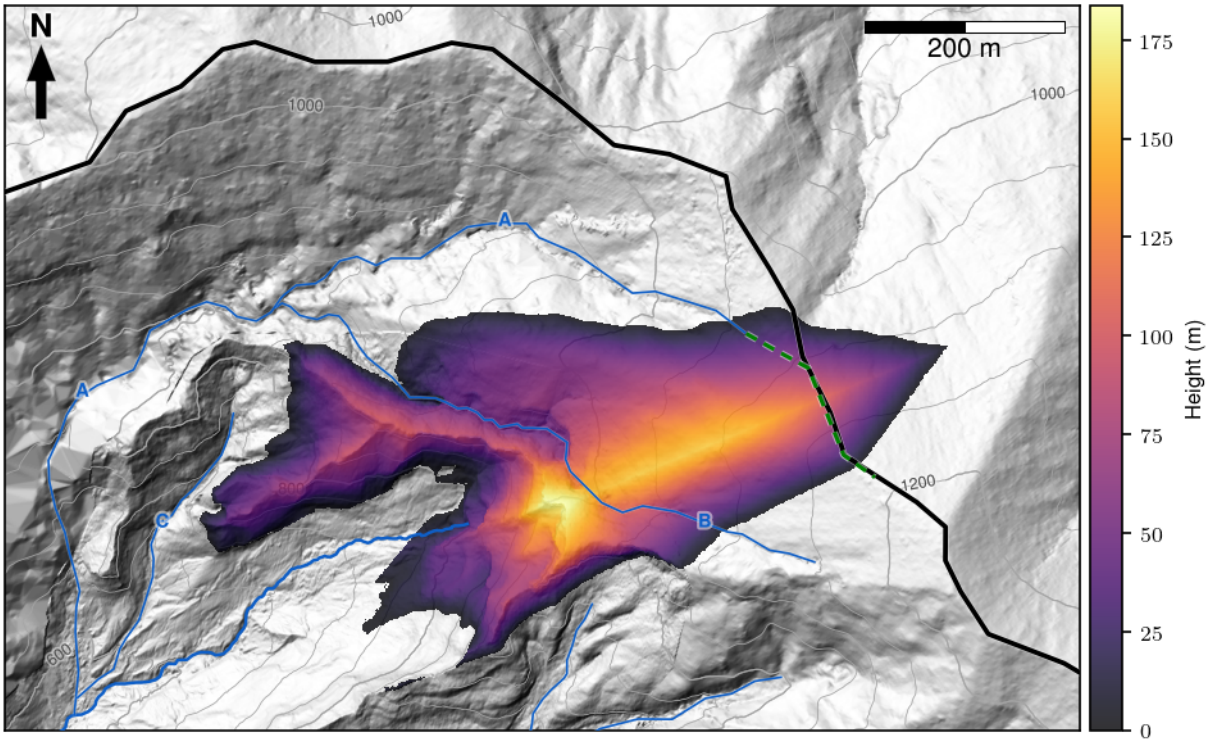

Figure 8. Potentially unstable volume. The height between the reconstructed basal surface (see Figure 7b) and the combined 07/2010-08/2018 DEM (displayed here) is given by the color scale. We only display heights above the contact between D and UPd units, and LPd and Upd units, and disregard heights below 1 m. The Samperre river (thick blue line), ravines (thin blue lines) and the Prêcheur destabilization structure (black line) are displayed as in Figure 1. The unstable volume is computed either directly, or by limiting the extent of the collapse (i) to ravine A continued along a topographic edge (green dashed line) or (ii) to ravine B (see Table 3).

Table 2. Surfaces used for quantifying a potential unstable volume, with characteristics of the associated best-fit planes. σ is the standard deviation of estimated dip and dip directions. See Appendix A for characteristic lengths and widths computations, and for the derivation of M and K. Following Fernández (2005), a good fit and reliability correspond to $M \geq 4$ and $K \leq 0.8$

	Description	dip (°)		azimuth (°)		RMS (m)	Characteristic length (m)	Characteristic width (m)	M	K
		mean	σ	mean	σ					
S1	*Co* outcrop visible in 2010	42.17	0.03	168.75	0.06	1.79	34.88	6.96	5.94	1.19
S2	*Co* outcrop visible in 2018	43.92	0.02	205.70	0.04	1.69	44.23	16.57	6.53	0.43
S3	*LPd* outcrop	47.32	0.02	308.00	0.01	7.23	161.76	29.90	6.21	1.19
S4[1]	Northern extent	57.32	n.a.	136.88	n.a.	n.a.	n.a.	n.a.	n.a.	n.a.
S5[1]	Southern rim	65.00	n.a.	318.00	n.a.	n.a.	n.a.	n.a.	n.a.	n.a.
S6	River bed	11.95	0.00	243.26	0.05	1.94	124.08	30.65	8.31	0.51

[1] Planes fitted manually to fit topographic trends

Table 3. Potentially unstable volumes in m^3. σ is the standard deviation of volume estimation, when considering the uncertainty on basal surface reconstruction (see Appendix A)

	Total volume (m^3)	South of ravine A (m^3)	South of ravine B (m^3)
Mean	8.3×10^6	7.9×10^6	3.5×10^6
σ	5.9×10^3	4.8×10^3	1.3×10^3

the Prêcheur river. Indeed, these deposits mainly correspond to screes remobilized at the Samperre cliff toe, and thus to collapsed materials from the *UPd* unit.

*In this context, it is more reasonable to rely on remote observations***Until complementary field work and geotechnical characterization are carried out, remote observations must be used**. For instance, the stability of units *Co* and *LPd* in coming years could be assessed by monitoring their evolution, *for instance* with yearly visual observations or topographic surveys. **In the mean time, limit equilibrium numerical models can help characterize the stability of the cliff by performing a sensitivity analysis on key parameters, including the geometry of the interfaces between geological units, the geotechnical properties of materials, and the presence and level of aquifers. In a first approach, simple 2D limit equilibrium models such as SSAP (Brunetti et al., 2014; Borselli, 2022) or FLAC/Slope (Itasca, 2022) could be tested.**

The stability of units *Co* may be questioned. Indeed its ochre colour suggests it has been extremely hydrothermal altered (e.g. Salaün et al., 2011), and many studies (e.g. Heap et al., 2021) have linked hydrothermal alteration to reduced rock stability. However, **after the 127 kyrs flank collapse,** alteration may have affected unit *Co* only at its surface. It is indeed a preferential flow path, as evidenced by water seepage at the interface between units *Co* and *UPd*. Besides, even if the unit is altered at greater depth, these water seepages suggest hydrothermal fluids no longer circulate within unit *Co*. *Hydrothermal activity certainly stopped 127 kyrs ago, when the first flank collapse deeply impacted the primitive volcanic edifice of Montagne Pelée.* Thus, we argue that the alteration of unit *Co* is old and has been compensated by (i) hydrothermal sealing, (ii) diagenetical cementation and (iii) lithostatic compaction (e.g. del Potro and Hürlimann, 2008). These three processes reduce connected porosity. For volcanic rocks, lower porosity is associated to increased cohesion and friction coefficient (Villeneuve and Heap, 2021). Thus, stability is increased, and the alteration of unit *Co* is compensated for. In turn, the surface of unit *Co* becomes a preferential sliding surface as observed for instance for old collapse scars on the Soufrière de Guadeloupe volcano (Salaün et al., 2011).

There is no clear sign of hydrothermal circulation within unit *LPd*, which limits possibility of both alteration and hydrothermal sealing. However, the proximity of the Montagne Pelée eruptive center suggests pyroclastic deposits of unit *LPd were***may have been** emplaced at relative high temperature, which favours welding (Quane and Russell, 2005). Then, as for unit *Co*, unit *LPd* was *certainly***likely** further strengthened by diagenetical cementing and lithostatic compaction. Furthermore, Boudon and Balcone-Boissard (2021) describe most of the pyroclastic deposits produced during this second stage as indured materials forming a succession of ridges particularly visible on the more eroded western flank of Montange Pelée edifice.

5.2 *Cliff destabilizations related to the drainage of a paleo-valley***Structural control of a valley paleo-surface on cliff destabilizations**

The correlation between paleo-morphology and volcanic flank collapse has been investigated in several studies. For instance, Branca and Ferrara (2013) relates past destabilizations of Etna volcano to the morphology of sedimentary units it grew on. Similarly, over the past 10 kyr, numerous flank collapses from the Soufrière de Guadeloupe volcano have occurred repeatedly in the collapse scar left by Morne Amic *event***flank collapse** (Komorowski et al., 2005; Rosas-Carbajal et al., 2016).

However, we could not find any study correlating directly destabilization of volcanic escarpments to the drainage of paleo-valleys **(i.e. the removal of solid materials filling the paleo-vallay)**, in tropical context or anywhere else. For instance, Branca (2003) analyze the successive filling and *drainage***emptying** phases of a fluvial valley affected by basaltic lava flows on Etna's flank, but do not associate it to destabilization episodes. **It may also be surprising that there are no other Samperre cliff like catchments on the flanks of Montagne Pelée volcano. A possible reason is that they have been eroded by surface water and/or subsequent small gravitational re-adjustments. Yet, the Samperre cliff catchment may also present some specifities, including the proximity of the Prêcheur collapse structure and the relative steep contact between *UPd* and underlying geological units. Geophysical surveys (e.g. AEM) on the Samperre cliff and other Pelée valleys would help further investigate this question.**

*T***In the mean time, t**he Réunion island (Indian ocean) might be a good candidate to find analogues of the Samperre cliff paleo-morphology. Indeed, Réunion island includes both an extinct and eroded volcanic center, the Piton des Neige, and an active volcano, the Piton de la Fournaise. An exemple of paleo-valley infilled by volcanic materials is the upper reach of the Rivière des Remparts (see figure 25.4 in Villeneuve et al., 2014). However, Piton des Neige and Piton de la Fournaise volcano have mainly erupted lava flows (Salvany et al., 2012; Chaput, 2013). Besides, Rault et al. (2022) suggest that most mass wasting events occurring in the Cirque of Salazie depression (associated to the dismantling of Piton des neiges volcano) are associated to the remobilization of old debris avalanches and epiclastic deposits (see also Chaput, 2013). As a result, destabilization mechanisms may differ from the Samperre cliff that is mainly composed of pyroclastic deposits.

Without any documented similar case studies, further data are needed to confirm or invalidate the hypothese that the destabilizations of the Samperre cliff are *linked to the drainage of a paleo-valleys made in this study***structurally controlled by the surface of a paleo-valley**. In this perspective, it will be important to analyze *of* future destabilization episodes, should they occur. In the mean time, the geometry of the paleo-valley could be constrained by geophysical surveys. Indeed, given observed water seepages, the contact between units *Co* and *UPd*, and *LPd* and *UPd*, is certainly associated to a permeability contrast, and thus a resistivity contrast (e.g. Romano et al., 2018; Huntley et al., 2019). *Indeed, o***O**lder volcanic formations often tend to have lower permeabilities as a result of filling of cavities and fractures (Singhal and Gupta, 2010), hydrothermal sealing (Polak et al., 2003) and compaction (Farquharson et al., 2017).

Given the difficulty to carry out terrestrial surveys in the Samperre cliff area, airborne electromagnetic surveys (AEM) are more feasible. They have already proven to provide valuable information to constrain landslides geometry (Nakazato and Konishi, 2005). Most of Martinique island was covered in 2013 by AEM surveys (Deparis et al., 2014; Coppo et al., 2015),

and the resulting data *was***were** used to investigate hydrogeological systems (Vittecoq et al., 2015, 2019) and active landslides (Thiery et al., 2017, 2021). This highlights the great potential of this method, but unfortunately the Samperre cliff could not be flown over in 2013. The current development of AEM drone-based survey could help acquiring AEM data on this zone. We expect the contrast between *Co* and *UPd* to be particularly clear, as these units clearly have different lithologies or degree of weathering (as evidenced by color variations). However, unit *LPd* and *UPd* are both pyroclastic deposits, hence the contrast may be less marked *but still identifiable because of the difference in age of deposition and consolidation*.

5.3 Volume estimation and implication for hazard assessment

The main surfaces controlling the extent of the reconstructed paleo-valley behind the cliff are *S2* and *S5*. The river bed (surface *S6*) has a very limited influence, because it lies below other surfaces, and in particular below *S1*, *S2* and *S3*. This is why it does not appear in Figure 7b). Similarly, surface**s** *S3 does***and *S4* do** not influence the final computed volume, provided we consider only unstable *volume***materials** in the Samperre cliff.

Our estimation of the uncertainty on the unstable volume is only related to the uncertainty on best-fit plane derivation. A more robust procedure should also take into account (i) the uncertainty on manual plane fitting for surfaces *S4* and *S5* and (ii) possible variations in structural orientations below the 08/2018 topography. In particular, we may expect the surface of unit *Co* to curve itself to the East, following the same trend as the Prêcheur destabilization structure, instead of keeping the orientation of surface *S2* (Figure 7b). This would be coherent with observations, as the dip direction of surfaces associated to unit *Co* gradually increases from the West to the East: N137°*E* for *S4*, N169°*E* for *S1* and N206°*E* for *S2* (see Figure 7 and Table 2).

Despite the lack of quantitative information, this possible bending of the interface between units *Co* and *UPd* can be taken into account, in a first approximation, if we simply delimit vertical surfaces constrained by topographic features. In a first case scenario, we assume that the paleo-valley did not extend further than the destabilization structure of the Prêcheur flank collapse. We thus use a North-East limit defined by ravine A (that follows the Prêcheur structure), continued along the ridge of the Prêcheur structure (green dashed line in Figure 8). The corresponding volume, 7.9×10^6 m^3, is of the same order than our first estimation (8.3×10^6 m^3) to within 5% difference. In a second more conservative scenario, we use ravine B (that runs behind Falaise Samperre) as North-East limit. The associated volume is 3.5×10^6 m^3.

The upper volume value 8×10^6 m^3 gives an estimation of the total rock mass volume that could be involved in future destabilization episodes, until the catchment reaches a long-term stability state. Given the collapsed volume between 2010 and 2018 (about 5×10^6 m^3), this equilibrium state may well be reached in the coming decades. However, this does not entail that hazard associated to lahars will be then reduced in the Prêcheur river. Indeed, solid materials remobilized by lahars could also come from multiple other sources, including lateral erosion from the banks of the Samperre river and fresh *euprive***eruptive** materials in the event of a new phreatic or magmatic eruption. Besides, although units *Co* and *LPd* are more stable than unit *UPd*, they may still be subjected to retrogressive erosion or gravitational *instablities***instabilities**. Finally, gravitational instabilities could also occur in adjacent gullies, in particular in ravine D where superficial instabilities were witnessed in 2019 (figure 2 in Peruzzetto, 2021a).

In comparison, the smaller volume value 3.5×10^6 m^3 is consistent with volumes destabilized in recent times (e.g., 2.1×10^6 m^3 in 2010 and 4.9×10^6 m^3 between 2010 and 2018) and could correspond to the volume of the next destabilization episode. **A more detailed estimation would require limit equilibrium 3D numerical modeling (Apuani et al., 2005; Reid et al., 2015; Verrucci et al., 2019; Heap et al., 2021), but more geotechnical data are needed to contrain simulations.** *It could collapse* **The next destabilization episode could occur** in a single event or, more likely, in a succession of smaller rock avalanches. In both cases, a significant scree reservoir will be formed at the toe of the Samperre cliff. The processes controlling its remobilization **by water** depend on factors that are hard to constrain in real-time monitoring, including precipitation intensities and pore-pressure within the reservoir. The resulting lahars may occur as a few major high-discharge events with the potential to flood the Prêcheur village downstream, as in 2010; or as multiple smaller but still dangerous events during a longer time period, which is highly disruptive for inhabitants, as in 2018. Our study suggests either of these crisis situations could still occur in the coming years, as a result destabilizations from the Samperre cliff. In the worst case scenario, we can consider a 3.5×10^6 m^3 reservoir created at the bottom of the cliff (neglecting bulking), and remobilized in a single lahar with solid fraction 75% (following classical solid fraction values as in Vallance and Iverson, 2015; Thouret et al., 2020). A rough estimation of the volume of the lahar is then 4.7×10^6 m^3. The associated damages would be very important. Indeed, using numerical simulations, Peruzzetto et al. (2022) showed that a 2.0×10^6 m^3 lahar has already the potential to flood a large part of the Prêcheur village.

However, in the current state of knowledge, it is impossible to predict the date of the next collapse and of the subsequent lahars: the physical processes controlling and triggering destabilizations on the Samperre cliff are difficult to constrain. Nevertheless, they are most likely associated with water circulations.

5.4 Destabilization mechanisms

As already suggested by Clouard et al. (2013) and Nachbaur et al. (2019) ground water circulations at the interface between units *Co* and *UPd* may be the main triggering factor for destabilizations. In the medium term (i.e. years), it could weaken the base of unit *UPd* by washing out fine particles. This suffusion process is widely documented in the litterature (e.g. Moffat et al., 2011; Wan and Fell, 2008; Prasomsri and Takahashi, 2021). Precipitations (and associated increased pore pressure) could be a triggering factor in the short-term, but only after a time lag allowing ground water to reach the cliff. Indeed, the 2018 destabilizations episodes started only 2 days after the major rainfall of Dec., 31 2017 (almost 150 mm in one day in the Prêcheur village Quefféléan, 2018). We do not have access to precipitations records for previous events.

Interestingly, the chronology of recent destabilization episodes suggest that weakening by ground water circulations is particularly important at the interface between units *Co* and *UPd*. Indeed, during the 2009-2010 destabilizations episode (Clouard et al., 2013), the first major collapses occurred on Aug. 19, 2009 on the North-West flank of the cliff (that is, in unit *UPd* above unit *Co*). The western and southern side then collapsed less than a year after, on May, 11. 2010. Similarly, ortho-photographs reveal that between 2010 and 2017, the cliff rim retreated to the north. The major 2018 destabilization episode concerned mainly the western side of the cliff (Figure 2a). Thus, we suggest destabilizations espiodes start on the North-West side of the cliff, at the interface between units *Co* and *UPd*, and progress to the East and South-East by successive retrogressive failures.

5.5 Contribution of rock avalanches to volcano dismantling

The volume detached from the Samperre cliff between March 2010 and July 2010 is about 2.1×10^6 m^3 (Clouard et al., 2013), and 4.9×10^6 m^3 between July 2010 and August 2018 (Quefféléan, 2018; Peruzzetto, 2021b; Peruzzetto et al., 2022). This yields an average volume of 0.9×10^6 m^3 yr^{-1}. This value certainly over-estimates the sediment production rate due to rock avalanches, because the 2018 collapse sequence was particularly large compared to previous episodes in 1998 or 2010. Quefféléan (2018) gives a rough estimation of the collapsed volume between 1951 and 2013 of $10-12 \times 10^6$ m^3, for an average sediment production of about $0.16-0.19 \times 10^6$ m^3 yr^{-1}. Considering that 15×10^6 m^3 collapsed between 1951 and 2018, we get a similar result: 0.22×10^6 m^3 yr^{-1}. It is twice as much as the estimation 0.1×10^6 m^3 yr^{-1} of Clouard et al. (2013). If we assume a density of 3000 kg m^3, we get a flux between 0.3 and 0.6 Mt yr^{-1}: it represents between 0.2% and 0.5% of the sediment flux from cliff retreat in Europe (over a distance of 127,000 km, see Regard et al., 2022).

In comparison, the total volume volumes involved in the Prêcheur and Rivière Sèche flank collapses is estimated between 27×10^9 m^3 (Germa et al., 2015) and 40×10^9 m^3 (Brunet et al., 2016). The associated long-time annual averages are 0.21×10^6 m^3 yr^{-1} and 0.31×10^6 m^3 yr^{-1}. Taking into account the on-land deposits of flank collapse, Germa et al. (2015) estimate a slightly lower rate of volume evacuated at sea by flank collapses: 0.15×10^6 m^3 yr^{-1}. All these rates are of the same order of magnitude as sediment production by rock avalanches from the Samperre cliff. **More refined comparisons are difficult because of the uncertainty on rate calculation**.

Of course, the Samperre cliff has been particularly active since (at least) 1950 and our results suggest it could reach an equilibrium state in the coming decades. Thus, the *extent to which the*associated sediment production rate *can be extended to longer time periods and to the whole Pelée edifice can be discussed***may over-estimate the actual sediment production rate linked to 10^6-10^7 m^3 landslides on the Pelée edifice over a long time period**. In particular, its specific location near the head-scarp of the Prêcheur collapse structure could enhance instabilities in comparison to other escarpments. *A*: as suggested by Germa et al. (2015), it is important to differentiate erosion rates inside and outside collapse calderas. However, the pyroclastic materials composing most of the cliff are, presumably, not specific to this site. Other outcrops are thus likely to be also eroded in the long-run by *smaller* landslides or runoff. This is particularly true in tropical islands where intense rainfalls favour superficial instabilities and erosion (e.g., more than 200 landslides cataloged in Martinique island between 2000 and 2020, Thiery et al., 2021). **Besides, our results are coherent with the conclusions of Brunetti et al. (2009). Indeed, using a global database of landslides, they find that landslide occurrence probability is proportional to $V^{-\beta}$, with V the landslide volume and $\beta = 1.1$ in volcanic context. Thus, the return period T_V is proportional to V^{β}. In turn, the sediment production rate V/T_V is proportional to $V^{(1-\beta)} = V^{-0.1}$. That is, the sediment production rate associated to landslides slightly decreases with landslide volume, or at least does not depend significantly on the landslide volume (given the uncertainties associated to the estimation of β).**

Thus, following Clouard et al. (2013), Germa et al. (2015) and Quartau et al. (2015), we suggest that the contribution of large edifice collapse to volcanic island dismantling is significant, but not necessarily dominant in comparison to other erosive processes**, and in particular smaller landslides**. Of course, this may depend on the geological context**, and the disctinction**

between processes is not easy as they can follow each other (e.g. surface water remobilizing landslide deposits). *and t*This question is still discussed in the literature. For instance, Salvany et al. (2012) argue that the the formation of volcanic cirques in the Réunion island (Indian Ocean) was mainly the result of regressive erosion by small landslides and runoff. On the contrary, Chaput (2013) suggests that the excavation of the cirques was first initiated by major gravitational instabilities, whose resulting breccias were then *eroded*remobilized by smaller landslides and surface water. More recently, Rault et al. (2022) estimate that landslides affecting both intact volcanic formations and epiclastic deposits and triggered by rainstorms have contributed to about 20% of the erosion of the Piton des Neiges over the last 72 kyrs.

In our view, the long-term role of intermediate landslides (i.e. between 10^6 and 10^7 m^3) should be further investigated. Indeed, landslides inventory often focus on smaller landslides or larger landslides, as can be clearly seen in figure 2 of Brunetti et al. (2009) giving the volume distribution of 19 landslide databases. Small landslides (below 10^6 m^3) are indeed more frequent and can be thus cataloged at the local or regional scale, from historic reports and field investigations. On the contrary, larger landslides inventories (above 10^8 m^3) are constructed from the geomorphological analysis of topographic surveys. Given the relative scarcity of such large landslides, large areas are investigated. At this scale, the footprint of intermediate landslides is less clear, such that their comprehensive and systematic identification is not easy. Future research on that matter and the construction of comprehensive ladslide databases in volcanic islands (e.g. Rault et al., 2022), would improve our understandings of erosion mechanisms in volcanic islands.

6 Conclusions

The quantification of unstable volumes in rocky cliffs in volcanic context is difficult because of the complex geometry of successive geological layers, especially when no geophysical, geotechnical or displacement data are available. In this study, we used historic aerial oblique photographs, ortho-rectified photographs, Digital Elevation Models and 3D point clouds to:

1. Identify geological units and characterize the geometry of deposition horizons, interfaces and outcrop surfaces,
2. *Identify stable and unstable geological units*Characterize the relative stability of geological units,
3. Reconstruct the paleo-morphology of the catchment, from which we deduced the 3D surface of a basal stable layer,
4. Quantify the potential unstable volume for future destabilizations.

We used the Samperre cliff (Martinique, Lesser Antilles) as a case study. Over the past decades it has produced several rock avalanches from 2 to 5×10^6 m^3, whose deposits can be remobilized as debris flows threatening the Prêcheur village, at the mouth of the Prêcheur river. From our observations and geometric characterization of geological units, we show that destabilizations of the Samperre cliff could be related to the *drainage of*remobilization old volcanic deposits that had filled a paleo-valley. We estimate the volume of materials still filling this paleo-valley to 7.9×10^6 m^3, and the volume involved in the next destabilization episodes to 3.5×10^6 m^3. These results are important for operational risk management.

Our interpretation that destabilizations are linked to *the drainage of*the presence of a paleo-valley could be verified or contradicted by airborne electro-magnetism surveys. They would identify, if it exists, the interface between the paleo-valley

and materials filling it. A regular monitoring of the cliff morphology during future destabilization episodes will also help better constrain long-term evolution scenarios. *More generally, our study contributes to quantify erosion rates in volcanic islands.* **Further field work should also be done in the future to identity and sample accessible outcrops of the geological units composing the Samperre cliff. This would allow to estimate the geotechnical properties of the materials that compose the cliff, and carry out limit equilibrium simulations.**

Data availability. The orthophotographs, DEMs, and photographs used to construct the photogrammetric models are not the property of the BRGM. Thus, they can't be made freely available. **Aerial pictures of the cliff, taken during helicopter flights, are provided in supplementary materials.**

Appendix A: Geometric analysis of points cloud

Provided a set of N points with coordinates $((X_1, Y_1, Z_1), ..., (X_N, Y_N, Z_N))$, we fit a plane of equation $aX + bY + cZ + d = 0$ to the corresponding cloud points through an ordinary least square regression, minimizing the distance between the points and the plane. The associated minimal Root Mean Square (RMS) is:

$$RMS = \left(\frac{1}{N} \sum_{i=1}^{i=N} (aX_i + bY_i + cZ_i + d)^2 \right)^{\frac{1}{2}}.$$

To characterize the robustness of the fit, we introduce the $(N \times 3)$ matrix M:

$$M = \begin{pmatrix} X_1 - E(X) & Y_1 - E(y) & Z_1 - E(Z) \\ \vdots & \vdots & \vdots \\ X_N - E(X) & Y_N - E(Y) & Z_N - E(Z) \end{pmatrix},$$

where $E(X)$, $E(Y)$ and $E(Z)$ are respectively the mean X, Y and Z coordinates of the point cloud. The (3×3) covariance matrix C is then given by:

$$C = \frac{1}{N} M^T M$$

The three positive eigen-values λ_1, λ_2 and λ_3, and associated eigen-vectors e_1, e_2, and e_3 help describe the geometry of the point cloud. Assuming $\lambda_1 \geq \lambda_2 \geq \lambda_3$, e_1 points in the direction of the cloud main axis, e_2 in the second main axis direction and e_3 in the third axis direction, all three axes being orthogonal to one another. The distribution of the points along these three axes is quantified by the eigen-values. For instance, if the points are aligned along a line, $\lambda_2 = \lambda_3 = 0$. If the points are homogeneously distributed on a disk, $\lambda_1 = \lambda_2$ and $\lambda_3 = 0$. In this perspective, $\sqrt{\lambda_1}$ can be seen as a characteristic length of the point cloud and $\sqrt{\lambda_2}$ as a characteristic width (see corresponding columns in Tables 2 and A1). More precisely, λ_1 and λ_2 are the variance of points projection on the first and second axes. λ_3 describes the points dispersion around the plane given by eigen-vectors e_1 and e_2: we have $\lambda_3 = RMS$.

For the plane fit to be robust, the RMS, i.e. λ_3, needs to be small in comparison to the length of the cloud. Following Fernández (2005), we use the indicator:

$$M = \ln(\lambda_1/\lambda_3)$$

The higher M is, the better the fit. To estimate the reliability of the plane orientation, we must assess the linearity of the point cloud, as multiple planes can fit a linear distribution of points, with similar RMS. Fernández (2005) suggest the indicator K:

$$K = \frac{\ln(\lambda_1/\lambda_2)}{\ln(\lambda_2/\lambda_3)}$$

The lower K is, the better the reliability of the fit. Low values of K are obtained if $\lambda_3 << \lambda_2$ (i.e. if the point cloud has a good degree of planarity) and/or if λ_1/λ_2 is close to 1 (by construction, $\lambda_1/\lambda_2 \geq 1$). Fernández (2005) run multiple numerical tests to estimate threshold values for M and K corresponding to good fit and reliability. They suggest we must have $M \geq 4$ and $K \leq 0.8$. In order to have a direct estimation of the uncertainty on dip and dip direction of the fitted plane, we use a bootstrap method. This is done by drawing randomly, with replacement, N points among the initial N points of the point cloud, and fitting a plane to the new point cloud. This procedure is repeated 100 times. The standard deviations of the resulting dip and dip directions are given in Table 2 and Table A1.

Author contributions. Conceptualization, Methodology and Validation M.P., Y.L., A.N., T.D.; Formal Analysis, Investigation and Visualization M.P., Y.L., A.N., T.D.; Resources and Data Curation M.P., Y.L., A.N., T.D.; Writing Original Draft Preparation M.P.; Writing Review & Editing M.P., Y.L., A.N., Y.T, C.L., T.D., B.V.; Supervision, Project Administration, and Funding Acquisition A.N., B.V, Y.L., Y.T, C.L.

Competing interests. The authors declare that they have no conflict of interest.

Acknowledgements. We gratefully thank the DGPR and DEAL Martinique for funding this research and the acquisition of topographic data. We also thank the staff of BRGM Martinique, BRGM Guadeloupe and OVSM-IPGP for their contribution to field work.

Table A1. Deposition horizons characterization. σ is the standard deviation of estimated dip and dip directions. See Appendix A for characteristic lengths and widths computations, and for the derivation of M and K. Following Fernández (2005), a good fit and reliability correspond to $M \geq 4$ and $K \leq 0.8$

Mean Altitude (m)	dip (°)		azimuth (°)		RMS (m)	Characteristic length (m)	Characteristic width (m)	M	K
	mean	σ	mean	σ					
723.54	19.06	0.27	269.49	0.27	2.29	64.57	15.24	6.68	0.76
749.86	23.01	0.21	258.46	0.13	0.80	40.91	7.51	7.88	0.76
764.67	13.22	0.25	242.55	4.14	0.84	25.62	2.70	6.84	1.92
766.42	**23.90**	**0.33**	**252.23**	**0.39**	**1.81**	**65.73**	**34.32**	**7.18**	**0.22**
792.50	17.00	0.29	262.14	0.78	0.84	36.03	7.21	7.51	0.75
795.30	14.92	1.14	267.31	5.88	0.73	23.75	1.36	6.96	4.64
813.17	9.82	0.11	291.63	1.42	0.40	31.46	3.44	8.72	1.03
821.96	15.27	0.17	263.26	0.92	0.27	22.41	2.17	8.82	1.12
832.81	6.98	0.23	219.50	3.42	0.33	13.32	2.46	7.38	0.84
843.32	10.13	0.13	232.06	1.01	0.31	20.87	3.91	8.41	0.66
847.60	5.85	0.08	291.39	5.59	0.23	15.82	1.39	8.49	1.34
854.92	5.43	0.20	252.21	1.41	0.47	32.83	5.25	8.50	0.76
864.34	10.83	0.28	257.05	1.33	0.49	23.70	3.60	7.78	0.94
875.21	23.33	1.19	210.64	1.02	0.39	8.99	1.79	6.25	1.07
915.00	14.29	1.71	267.02	2.01	0.32	10.40	0.76	6.96	3.00
932.54	17.87	0.88	229.60	0.87	0.21	9.65	1.18	7.66	1.22

References

Apuani, T., Corazzato, C., Cancelli, A., and Tibaldi, A.: Stability of a Collapsing Volcano (Stromboli, Italy): Limit Equilibrium Analysis and Numerical Modelling, Journal of Volcanology and Geothermal Research, 144, 191–210, https://doi.org/10.1016/j.jvolgeores.2004.11.028, 2005.

Aubaud, C., Athanase, J.-E., Clouard, V., Barras, A.-V., and Sedan, O.: A Review of Historical Lahars, Floods, and Landslides in the Precheur River Catchment (Montagne Pelee Volcano, Martinique Island, Lesser Antilles), Bulletin de la Societe Geologique de France, 184, 137–154, https://doi.org/10.2113/gssgfbull.184.1-2.137, 2013.

Belle, P., Aunay, B., Bernardie, S., Grandjean, G., Ladouche, B., Mazué, R., and Join, J.-L.: The Application of an Innovative Inverse Model for Understanding and Predicting Landslide Movements (Salazie Cirque Landslides, Reunion Island), Landslides, 11, 343–355, https://doi.org/10.1007/s10346-013-0393-5, 2014.

Blahůt, J., Balek, J., Klimeš, J., Rowberry, M., Kusák, M., and Kalina, J.: A Comprehensive Global Database of Giant Landslides on Volcanic Islands, Landslides, https://doi.org/10.1007/s10346-019-01275-8, 2019.

Borselli, L.: SSAP, https://ssap.eu, 2022.

Boudon, G. and Balcone-Boissard, H.: Volcanological Evolution of Montagne Pelée (Martinique): A Textbook Case of Alternating Plinian and Dome-Forming Eruptions, Earth-Science Reviews, 221, 103 754, https://doi.org/10.1016/j.earscirev.2021.103754, 2021.

Boudon, G., Le Friant, A., Villemant, B., Viodé, J.-P., Anténor-Habazac, C., and Hammmouya, G.: Volcanic Hazard Atlas of the Lesser Antilles : Martinique, in: Volcanic Hazard Atlas of the Lesser Antilles, edited by Lindsay, J., Robertson, R., Shepherd, J., and Ali, S., pp. 126–145, University of the West Indies, Seismic Research Unit, Trinidad and IAVCEI, 2005.

Boudon, G., Le Friant, A., Komorowski, J.-C., Deplus, C., and Semet, M. P.: Volcano Flank Instability in the Lesser Antilles Arc: Diversity of Scale, Processes, and Temporal Recurrence, Journal of Geophysical Research, 112, B08 205, https://doi.org/10.1029/2006JB004674, 2007.

Branca, S.: Geological and Geomorphological Evolution of the Etna Volcano NE Flank and Relationships between Lava Flow Invasions and Erosional Processes in the Alcantara Valley (Italy), Geomorphology, 53, 247–261, https://doi.org/10.1016/S0169-555X(02)00315-X, 2003.

Branca, S. and Ferrara, V.: The Morphostructural Setting of Mount Etna Sedimentary Basement (Italy): Implications for the Geometry and Volume of the Volcano and Its Flank Instability, Tectonophysics, 586, 46–64, https://doi.org/10.1016/j.tecto.2012.11.011, 2013.

Brunet, M., Le Friant, A., Boudon, G., Lafuerza, S., Talling, P., Hornbach, M., Ishizuka, O., Lebas, E., Guyard, H., and Party, I. E. . S.: Composition, Geometry, and Emplacement Dynamics of a Large Volcanic Island Landslide Offshore Martinique: From Volcano Flank-Collapse to Seafloor Sediment Failure?, Geochemistry, Geophysics, Geosystems, 17, 699–724, https://doi.org/10.1002/2015GC006034, 2016.

Brunet, M., Moretti, L., Le Friant, A., Mangeney, A., Fernández Nieto, E. D., and Bouchut, F.: Numerical Simulation of the 30–45 Ka Debris Avalanche Flow of Montagne Pelée Volcano, Martinique: From Volcano Flank Collapse to Submarine Emplacement, Natural Hazards, 87, 1189–1222, https://doi.org/10.1007/s11069-017-2815-5, 2017.

Brunetti, M. T., Guzzetti, F., and Rossi, M.: Probability Distributions of Landslide Volumes, Nonlinear Processes in Geophysics, 16, 179–188, https://doi.org/10.5194/npg-16-179-2009, 2009.

Brunetti, M. T., Guzzetti, F., Cardinali, M., Fiorucci, F., Santangelo, M., Mancinelli, P., Komatsu, G., and Borselli, L.: Analysis of a New Geomorphological Inventory of Landslides in Valles Marineris, Mars, Earth and Planetary Science Letters, 405, 156–168, https://doi.org/10.1016/j.epsl.2014.08.025, 2014.

Buckley, S. J., Ringdal, K., Naumann, N., Dolva, B., Kurz, T. H., Howell, J. A., and Dewez, T. J.: LIME: Software for 3-D Visualization, Interpretation, and Communication of Virtual Geoscience Models, Geosphere, 15, 222–235, https://doi.org/10.1130/GES02002.1, 2019.

Carazzo, G., Tait, S., Kaminski, E., and Gardner, J. E.: The Recent Plinian Explosive Activity of Mt. Pelée Volcano (Lesser Antilles): The P1 AD 1300 Eruption, Bulletin of Volcanology, 74, 2187–2203, https://doi.org/10.1007/s00445-012-0655-4, 2012.

Carazzo, G., Tait, S., Michaud-Dubuy, A., Fries, A., and Kaminski, E.: Transition from Stable Column to Partial Collapse during the 79 Cal CE P3 Plinian Eruption of Mt. Pelée Volcano (Lesser Antilles), Journal of Volcanology and Geothermal Research, 392, 106 764, https://doi.org/10.1016/j.jvolgeores.2019.106764, 2020.

Chaput, M.: Déformation et activité intrusive des volcans boucliers - Du terrain à la modélisation numérique (Piton des Neiges, La Réunion), Ph.D. thesis, Université de la Réunion, 2013.

Clouard, V., Athanase, J.-E., and Aubaud, C.: Physical Characteristics and Triggering Mechanisms of the 2009-2010 Landslide Crisis at Montagne Pelee Volcano, Martinique: Implication for Erosional Processes and Debris-Flow Hazards, Bulletin de la Societe Geologique de France, 184, 155–164, https://doi.org/10.2113/gssgfbull.184.1-2.155, 2013.

CloudCompare: GPL Software, Version 2.11.3, 2020.

Coppo, N., Baltassat, J.-M., Girard, J.-F., Wawrzyniak, P., Hautot, S., Tarits, P., Jacob, T., Martelet, G., Mathieu, F., Gadalia, A., Bouchot, V., and Traineau, H.: 3-D Magnetotelluric Investigations for Geothermal Exploration in Martinique (Lesser Antilles). Characteristic Deep Resistivity Structures, and Shallow Resistivity Distribution Matching Heliborne TEM Results, arXiv:1501.06541 [physics], 2015.

Coviello, V., Capra, L., Norini, G., Dávila, N., Ferrés, D., Márquez-Ramírez, V. H., and Pico, E.: Earthquake-Induced Debris Flows at Popocatépetl Volcano, Mexico, Earth Surface Dynamics, 9, 393–412, https://doi.org/10.5194/esurf-9-393-2021, 2021.

Cutler, K. S., Watt, S. F. L., Cassidy, M., Madden-Nadeau, A. L., Engwell, S. L., Abdurrachman, M., Nurshal, M. E. M., Tappin, D. R., Carey, S. N., Novellino, A., Hayer, C., Hunt, J. E., Day, S. J., Grilli, S. T., Kurniawan, I. A., and Kartadinata, N.: Downward-Propagating Eruption Following Vent Unloading Implies No Direct Magmatic Trigger for the 2018 Lateral Collapse of Anak Krakatau, Earth and Planetary Science Letters, 578, 117 332, https://doi.org/10.1016/j.epsl.2021.117332, 2022.

De Rita, D., Giordano, G., and Milli, S.: Forestepping-Backstepping Stacking Pattern of Volcaniclastic Successions: Roccamonfina Volcano, Italy, Journal of Volcanology and Geothermal Research, 78, 267–288, https://doi.org/10.1016/S0377-0273(97)00005-X, 1997.

del Potro, R. and Hürlimann, M.: Geotechnical Classification and Characterisation of Materials for Stability Analyses of Large Volcanic Slopes, Engineering Geology, 98, 1–17, https://doi.org/10.1016/j.enggeo.2007.11.007, 2008.

Deparis, J., Reninger, P.-A., Perrin, J., Martelet, G., and Audru, J.-C.: Acquisition géophysique héliportée électromagnétique de la Matinique, Public report BRGM/RP-62428-FR, BRGM, Orléans, France, 2014.

Di Traglia, F., Fornaciai, A., Favalli, M., Nolesini, T., and Casagli, N.: Catching Geomorphological Response to Volcanic Activity on Steep Slope Volcanoes Using Multi-Platform Remote Sensing, Remote Sensing, 12, 438, https://doi.org/10.3390/rs12030438, 2020.

Durand, V., Mangeney, A., Haas, F., Jia, X., Bonilla, F., Peltier, A., Hibert, C., Ferrazzini, V., Kowalski, P., Lauret, F., Brunet, C., Satriano, C., Wegner, K., Delorme, A., and Villeneuve, N.: On the Link Between External Forcings and Slope Instabilities in the Piton de La Fournaise Summit Crater, Reunion Island, Journal of Geophysical Research: Earth Surface, 123, 2422–2442, https://doi.org/10.1029/2017JF004507, 2018.

Farquharson, J. I., Baud, P., and Heap, M. J.: Inelastic Compaction and Permeability Evolution in Volcanic Rock, Solid Earth, 8, 561–581, https://doi.org/10.5194/se-8-561-2017, 2017.

Fernández, O.: Obtaining a Best Fitting Plane through 3D Georeferenced Data, Journal of Structural Geology, 27, 855–858, https://doi.org/10.1016/j.jsg.2004.12.004, 2005.

Germa, A., Quidelleur, X., Lahitte, P., Labanieh, S., and Chauvel, C.: The K–Ar Cassignol–Gillot Technique Applied to Western Martinique Lavas: A Record of Lesser Antilles Arc Activity from 2Ma to Mount Pelée Volcanism, Quaternary Geochronology, 6, 341–355, https://doi.org/10.1016/j.quageo.2011.02.001, 2011.

Germa, A., Lahitte, P., and Quidelleur, X.: Construction and Destruction of Mont Pelée Volcano: Volumes and Rates Constrained from a Geomorphological Model of Evolution, Journal of Geophysical Research: Earth Surface, 120, 1206–1226, https://doi.org/10.1002/2014JF003355, 2015.

Guthrie, R. H., Friele, P., Allstadt, K., Roberts, N., Evans, S. G., Delaney, K. B., Roche, D., Clague, J. J., and Jakob, M.: The 6 August 2010 Mount Meager Rock Slide-Debris Flow, Coast Mountains, British Columbia: Characteristics, Dynamics, and Implications for Hazard and Risk Assessment, Natural Hazards and Earth System Sciences, 12, 1277–1294, https://doi.org/10.5194/nhess-12-1277-2012, 2012.

Hamada, A. and Toramaru, A.: Analogue Experiments on Morphological Transition from Colonnade to Entablature of Columnar Joints, Journal of Volcanology and Geothermal Research, 402, 106 979, https://doi.org/10.1016/j.jvolgeores.2020.106979, 2020.

Harnett, C. E., Thomas, M. E., Calder, E. S., Ebmeier, S. K., Telford, A., Murphy, W., and Neuberg, J.: Presentation and Analysis of a Worldwide Database for Lava Dome Collapse Events: The Global Archive of Dome Instabilities (GLADIS), Bulletin of Volcanology, 81, 16, https://doi.org/10.1007/s00445-019-1276-y, 2019.

Heap, M. J., Baumann, T. S., Rosas-Carbajal, M., Komorowski, J.-C., Gilg, H. A., Villeneuve, M., Moretti, R., Baud, P., Carbillet, L., Harnett, C., and Reuschlé, T.: Alteration-Induced Volcano Instability at La Soufrière de Guadeloupe (Eastern Caribbean), Journal of Geophysical Research: Solid Earth, 126, e2021JB022 514, https://doi.org/10.1029/2021JB022514, 2021.

Hickey, J., Lloyd, R., Biggs, J., Arnold, D., Mothes, P., and Muller, C.: Rapid Localized Flank Inflation and Implications for Potential Slope Instability at Tungurahua Volcano, Ecuador, Earth and Planetary Science Letters, 534, 116 104, https://doi.org/10.1016/j.epsl.2020.116104, 2020.

Humbert, M., Pasquet, R., and Stieltjes, L.: Les Risques Géologiques Dans Les Cirques de Salazie et de Cilaos (Ile de La Réunion), Tech. Rep. 81 SGN 543 GEG-REU, BRGM, 1981.

Huntley, D., Bobrowsky, P., Hendry, M., Macciotta, R., and Best, M.: Multi-Technique Geophysical Investigation of a Very Slow-moving Landslide near Ashcroft, British Columbia, Canada, Journal of Environmental and Engineering Geophysics, 24, 87–110, https://doi.org/10.2113/JEEG24.1.87, 2019.

IGN: BD ORTHO | Géoservices, https://geoservices.ign.fr/documentation/donnees/ortho/bdortho, 2021a.

IGN: BD ORTHO Historique | Géoservices, https://geoservices.ign.fr/documentation/donnees/ortho/bdorthohisto, 2021b.

INSEE: Données Carroyées – Niveau Naturel, https://www.insee.fr/fr/statistiques/4176281?sommaire=4176305, 2015.

Itasca: FLAC/Slope, Itasca, https://www.itascacg.com/software/FLAC-Slope, 2022.

Jaboyedoff, M., Chigira, M., Arai, N., Derron, M.-H., Rudaz, B., and Tsou, C.-Y.: Testing a Failure Surface Prediction and Deposit Reconstruction Method for a Landslide Cluster That Occurred during Typhoon Talas (Japan), Earth Surface Dynamics, 7, 439–458, https://doi.org/10.5194/esurf-7-439-2019, 2019.

Jaboyedoff, M., Dario, C., Marc-Henri, D., Thierry, O., Ivanna Marina, P., and Bejamin, R.: A Review of Methods Used to Estimate Initial Landslide Failure Surface Depths and Volumes, Engineering Geology, 267, 105 478, https://doi.org/10.1016/j.enggeo.2020.105478, 2020.

Komorowski, J.-C., Boudon, G., Semet, M., Beauducel, F., Anténor-Habazac, C., Bazin, S., and Hammmouya, G.: Volcanic Hazard Atlas of the Lesser Antilles : Guadeloupe, in: Volcanic Hazard Atlas of the Lesser Antilles, edited by Lindsay, J., Robertson, R., Shepherd, J., and Ali, S., pp. 65–102, University of the West Indies, Seismic Research Unit, Trinidad and IAVCEI, 2005.

Lavigne, F., Degeai, J.-P., Komorowski, J.-C., Guillet, S., Robert, V., Lahitte, P., Oppenheimer, C., Stoffel, M., Vidal, C. M., Surono, Pratomo, I., Wassmer, P., Hajdas, I., Hadmoko, D. S., and de Belizal, E.: Source of the Great A.D. 1257 Mystery Eruption Unveiled, Samalas Volcano, Rinjani Volcanic Complex, Indonesia, Proceedings of the National Academy of Sciences, 110, 16 742–16 747, https://doi.org/10.1073/pnas.1307520110, 2013.

Le Friant, A., Boudon, G., Deplus, C., and Villemant, B.: Large-Scale Flank Collapse Events during the Activity of Montagne Pelée, Martinique, Lesser Antilles, Journal of Geophysical Research: Solid Earth, 108, 2055, https://doi.org/10.1029/2001JB001624, 2003.

Legendre, Y.: Reconstruction Fine de l'histoire Éruptive et Scenarii Éruptifs à La Soufrière de Guadeloupe : Vers Un Modèle Intégré de Fonctionnement Du Volcan, Thesis, Paris 7, 2012.

Lim, C., Huh, M., Yi, K., and Lee, C.: Genesis of the Columnar Joints from Welded Tuff in Mount Mudeung National Geopark, Republic of Korea, Earth, Planets and Space, 67, 152, https://doi.org/10.1186/s40623-015-0323-y, 2015.

Manville, V., Németh, K., and Kano, K.: Source to Sink: A Review of Three Decades of Progress in the Understanding of Volcaniclastic Processes, Deposits, and Hazards, Sedimentary Geology, 220, 136–161, https://doi.org/10.1016/j.sedgeo.2009.04.022, 2009.

Mathon, C. and Barras, A.: Risque d'occurence de Lave Torrentielle Dans La Rivière Du Prêcheur Suite à l'éboulement Du 11 Mai 2010, Rapport d'expertise BRGM/RP - 58697-FR, BRGM, 2010.

Maury, R. C., Westbrook, G. K., Baker, P. E., Bouysse, P., and Westercamp, D.: Geology of the Lesser Antilles, in: The Caribbean Region, vol. H, Geological Society of America, Boulder, CO, 1991.

McDougall, S.: 2014 Canadian Geotechnical Colloquium: Landslide Runout Analysis — Current Practice and Challenges, Canadian Geotechnical Journal, 54, 605–620, https://doi.org/10.1139/cgj-2016-0104, 2017.

Mitchell, A., McDougall, S., Nolde, N., Brideau, M.-A., Whittall, J., and Aaron, J. B.: Rock Avalanche Runout Prediction Using Stochastic Analysis of a Regional Dataset, Landslides, https://doi.org/10.1007/s10346-019-01331-3, 2019.

Moffat, R., Fannin, R. J., and Garner, S. J.: Spatial and Temporal Progression of Internal Erosion in Cohesionless Soil, Canadian Geotechnical Journal, 48, 399–412, https://doi.org/10.1139/T10-071, 2011.

Moretti, L., Allstadt, K., Mangeney, A., Capdeville, Y., Stutzmann, E., and Bouchut, F.: Numerical Modeling of the Mount Meager Landslide Constrained by Its Force History Derived from Seismic Data, Journal of Geophysical Research: Solid Earth, 120, 2579–2599, https://doi.org/10.1002/2014JB011426, 2015.

Nachbaur, A., Legendre, Y., Lombard, M., and Dewez, T.: Caractérisation Géologique et Identification Des Mécanismes d'instabilité de La Falaise Samperre, Rapport Final RP-68564-FR, BRGM, 2019.

Nakazato, H. and Konishi, N.: Subsurface Structure Exploration of Wide Landslide Area by Aerial Electromagnetic Exploration, Landslides, 2, 165–169, https://doi.org/10.1007/s10346-005-0056-2, 2005.

NGU: Recommended Hazard and Risk Classification System for Large Unstable Rock Slopes in Norway, Tech. Rep. 2012.029, Geological Survey of Norway, 2012.

Pavlis, T. L. and Mason, K. A.: The New World of 3D Geologic Mapping, GSA Today, pp. 4–10, https://doi.org/10.1130/GSATG313A.1, 2017.

Peruzzetto, M.: Modélisation de scénarios de déstabilisation de la Falaise Samperre et de propagation des lahars, Rapport final BRGM/RP-71149-FR, BRGM, Orléans, France, 2021a.

Peruzzetto, M.: Numerical Modeling of Dry and Water-Laden Gravitational Flows for Quantitative Hazard Assessment, Ph.D. thesis, Université de Paris, 2021b.

Peruzzetto, M., Komorowski, J.-C., Friant, A. L., Rosas-Carbajal, M., Mangeney, A., and Legendre, Y.: Modeling of Partial Dome Collapse of La Soufrière of Guadeloupe Volcano: Implications for Hazard Assessment and Monitoring, Scientific Reports, 9, 1–15, https://doi.org/10.1038/s41598-019-49507-0, 2019.

Peruzzetto, M., Mangeney, A., Grandjean, G., Levy, C., Thiery, Y., Rohmer, J., and Lucas, A.: Operational Estimation of Landslide Runout: Comparison of Empirical and Numerical Methods, Geosciences, 10, 424, https://doi.org/10.3390/geosciences10110424, 2020.

Peruzzetto, M., Levy, C., Thiery, Y., Grandjean, G., Mangeney, A., Lejeune, A.-M., Nachbaur, A., Legendre, Y., Vittecoq, B., Saurel, J.-M., Clouard, V., Dewez, T., Fontaine, F. R., Mergili, M., Lagarde, S., Komorowski, J.-C., Le Friant, A., and Lemarchand, A.: Simplified Simulation of Rock Avalanches and Subsequent Debris Flows with a Single Thin-Layer Model: Application to the Prêcheur River (Martinique, Lesser Antilles), Engineering Geology, 296, 106 457, https://doi.org/10.1016/j.enggeo.2021.106457, 2022.

Polak, A., Elsworth, D., Yasuhara, H., Grader, A. S., and Halleck, P. M.: Permeability Reduction of a Natural Fracture under Net Dissolution by Hydrothermal Fluids, Geophysical Research Letters, 30, https://doi.org/10.1029/2003GL017575, 2003.

Prasomsri, J. and Takahashi, A.: Experimental Study on Suffusion under Multiple Seepages and Its Impact on Undrained Mechanical Responses of Gap-Graded Soil, Soils and Foundations, 61, 1660–1680, https://doi.org/10.1016/j.sandf.2021.10.003, 2021.

Quane, S. L. and Russell, J. K.: Ranking Welding Intensity in Pyroclastic Deposits, Bulletin of Volcanology, 67, 129–143, https://doi.org/10.1007/s00445-004-0367-5, 2005.

Quartau, R., Hipólito, A., Mitchell, N. C., Gaspar, J. L., and Brandão, F.: Comment on "Construction and Destruction of a Volcanic Island Developed inside an Oceanic Rift: Graciosa Island, Terceira Rift, Azores" by Sibrant et al. (2014) and Proposal of a New Model for Graciosa's Geological Evolution, Journal of Volcanology and Geothermal Research, 303, 146–156, https://doi.org/10.1016/j.jvolgeores.2015.07.007, 2015.

Quefféléan, Y.: Mission d'expertise ONF-RTM Sur Les Lahars Du Prêcheur, Appui tehcnique DGPR, ONF-RTM, 2018.

Ramalho, R. S., Quartau, R., Trenhaile, A. S., Mitchell, N. C., Woodroffe, C. D., and Ávila, S. P.: Coastal Evolution on Volcanic Oceanic Islands: A Complex Interplay between Volcanism, Erosion, Sedimentation, Sea-Level Change and Biogenic Production, Earth-Science Reviews, 127, 140–170, https://doi.org/10.1016/j.earscirev.2013.10.007, 2013.

Rault, C., Thiery, Y., Chaput, M., Reninger, P. A., Dewez, T. J. B., Michon, L., Samyn, K., and Aunay, B.: Landslide Processes Involved in Volcano Dismantling From Past to Present: The Remarkable Open-Air Laboratory of the Cirque de Salazie (Reunion Island), Journal of Geophysical Research: Earth Surface, 127, e2021JF006 257, https://doi.org/10.1029/2021JF006257, 2022.

Regard, V., Prémaillon, M., Dewez, T. J. B., Carretier, S., Jeandel, C., Godderis, Y., Bonnet, S., Schott, J., Pedoja, K., Martinod, J., Viers, J., and Fabre, S.: Rock Coast Erosion: An Overlooked Source of Sediments to the Ocean. Europe as an Example, Earth and Planetary Science Letters, 579, 117 356, https://doi.org/10.1016/j.epsl.2021.117356, 2022.

Reid, M. E.: Massive Collapse of Volcano Edifices Triggered by Hydrothermal Pressurization, Geology, 32, 373–376, https://doi.org/10.1130/G20300.1, 2004.

Reid, M. E., Christian, S. B., Brien, D. L., and Henderson, S. T.: Scoops3D—Software to Analyze Three-Dimensional Slope Stability Throughout a Digital Landscape, in: Landslide and Debris-Flow Assessment, vol. 14 of *Techniques and Methods*, 2015.

Revil, A., Coperey, A., Heap, M. J., and Carbillet, L.: A Geophysical Index to Map Alteration, Permeability, and Mechanical Properties within Volcanoes. Application to the Soft Volcanic Rocks from Whakaari/White Island (New Zealand), Journal of Volcanology and Geothermal Research, 401, 106 945, https://doi.org/10.1016/j.jvolgeores.2020.106945, 2020.

Romano, G., Balasco, M., Siniscalchi, A., Gueguen, E., Petrillo, Z., and Tripaldi, S.: Geological and Geo-Structural Characterization of the Montemurro Area (Southern Italy) Inferred from Audiomagnetotelluric Survey, Geomatics, Natural Hazards and Risk, 9, 1156–1171, https://doi.org/10.1080/19475705.2018.1502210, 2018.

Rosas-Carbajal, M., Komorowski, J.-C., Nicollin, F., and Gibert, D.: Volcano Electrical Tomography Unveils Edifice Collapse Hazard Linked to Hydrothermal System Structure and Dynamics, Scientific Reports, 6, https://doi.org/10.1038/srep29899, 2016.

Rosas-Carbajal, M., Jourde, K., Marteau, J., Deroussi, S., Komorowski, J.-C., and Gibert, D.: Three-Dimensional Density Structure of La Soufrière de Guadeloupe Lava Dome from Simultaneous Muon Radiographies and Gravity Data: 3-D MUON TOMOGRAPHY OF LA SOUFRIÈRE, Geophysical Research Letters, 44, 6743–6751, https://doi.org/10.1002/2017GL074285, 2017.

Salaün, A., Villemant, B., Gérard, M., Komorowski, J.-C., and Michel, A.: Hydrothermal Alteration in Andesitic Volcanoes: Trace Element Redistribution in Active and Ancient Hydrothermal Systems of Guadeloupe (Lesser Antilles), Journal of Geochemical Exploration, 3, 59–83, https://doi.org/10.1016/j.gexplo.2011.06.004, 2011.

Salvany, T., Lahitte, P., Nativel, P., and Gillot, P.-Y.: Geomorphic Evolution of the Piton Des Neiges Volcano (Réunion Island, Indian Ocean): Competition between Volcanic Construction and Erosion since 1.4Ma, Geomorphology, 136, 132–147, https://doi.org/10.1016/j.geomorph.2011.06.009, 2012.

Schaefer, L. N., Di Traglia, F., Chaussard, E., Lu, Z., Nolesini, T., and Casagli, N.: Monitoring Volcano Slope Instability with Synthetic Aperture Radar: A Review and New Data from Pacaya (Guatemala) and Stromboli (Italy) Volcanoes, Earth-Science Reviews, 192, 236–257, https://doi.org/10.1016/j.earscirev.2019.03.009, 2019.

Scott, K. M., Vallance, J. W., Kerle, N., Macías, J. L., Strauch, W., and Devoli, G.: Catastrophic Precipitation-Triggered Lahar at Casita Volcano, Nicaragua: Occurrence, Bulking and Transformation, Earth Surface Processes and Landforms, 30, 59–79, https://doi.org/10.1002/esp.1127, 2005.

Siebert, L.: Large Volcanic Debris Avalanches: Characteristics of Source Areas, Deposits, and Associated Eruptions, Journal of Volcanology and Geothermal Research, 22, 163–197, https://doi.org/10.1016/0377-0273(84)90002-7, 1984.

Siebert, L., Glicken, H., and Ui, T.: Volcanic Hazards from Bezymianny- and Bandai-type Eruptions, Bulletin of Volcanology, 49, 435–459, https://doi.org/10.1007/BF01046635, 1987.

Singhal, B. B. S. and Gupta, R. P.: Hydrogeology of Volcanic Rocks, in: Applied Hydrogeology of Fractured Rocks: Second Edition, edited by Singhal, B. and Gupta, R., pp. 257–268, Springer Netherlands, Dordrecht, https://doi.org/10.1007/978-90-481-8799-7_14, 2010.

Solaro, C., Boudon, G., Le Friant, A., Balcone-Boissard, H., Emmanuel, L., and Paterne, M.: New Insights into the Recent Eruptive and Collapse History of Montagne Pelée (Lesser Antilles Arc) from Offshore Marine Drilling Site U1401A (IODP Expedition 340), Journal of Volcanology and Geothermal Research, 403, 107 001, https://doi.org/10.1016/j.jvolgeores.2020.107001, 2020.

Stothers, R. B.: The Great Tambora Eruption in 1815 and Its Aftermath, Science, 224, 1191–1198, https://doi.org/10.1126/science.224.4654.1191, 1984.

Thiele, S. T., Grose, L., Samsu, A., Micklethwaite, S., Vollgger, S. A., and Cruden, A. R.: Rapid, Semi-Automatic Fracture and Contact Mapping for Point Clouds, Images and Geophysical Data, Solid Earth, 8, 1241–1253, https://doi.org/10.5194/se-8-1241-2017, 2017.

Thiery, Y., Reninger, P.-A., Lacquement, F., Raingeard, A., Lombard, M., and Nachbaur, A.: Analysis of Slope Sensitivity to Landslides by a Transdisciplinary Approach in the Framework of Future Development: The Case of La Trinité in Martinique (French West Indies), Geosciences, 7, 135, https://doi.org/10.3390/geosciences7040135, 2017.

Thiery, Y., Reninger, P.-A., and Nachbaur, A.: Airborne Electromagnetics to Improve Landslide Knowledge in Tropical Volcanic Environments, Applied Sciences, 11, 3390, https://doi.org/10.3390/app11083390, 2021.

Thouret, J. C.: Volcanic Geomorphology—an Overview, Earth-Science Reviews, 47, 95–131, https://doi.org/10.1016/S0012-8252(99)00014-8, 1999.

Thouret, J. C., Antoine, S., Magill, C., and Ollier, C.: Lahars and Debris Flows: Characteristics and Impacts, Earth-Science Reviews, 201, 103 003, https://doi.org/10.1016/j.earscirev.2019.103003, 2020.

Vallance, J. W. and Iverson, R. M.: Lahars and Their Deposits, in: The Encyclopedia of Volcanoes, pp. 649–664, Academic Press, Amsterdam, second edition edn., https://doi.org/10.1016/B978-0-12-385938-9.00037-7, 2015.

van Wyk de Vries, B., Kerle, N., and Petley, D.: Sector Collapse Forming at Casita Volcano, Nicaragua, Geology, 28, 167–170, https://doi.org/10.1130/0091-7613(2000)28<167:SCFACV>2.0.CO;2, 2000.

Verrucci, L., Tommasi, P., Boldini, D., Graziani, A., and Rotonda, T.: Modelling the Instability Phenomena on the NW Flank of Stromboli Volcano (Italy) Due to Lateral Dyke Intrusion, Journal of Volcanology and Geothermal Research, 371, 245–262, https://doi.org/10.1016/j.jvolgeores.2019.01.007, 2019.

Villeneuve, M. C. and Heap, M. J.: Calculating the Cohesion and Internal Friction Angle of Volcanic Rocks and Rock Masses, Volcanica, 4, 279–293, https://doi.org/10.30909/vol.04.02.279293, 2021.

Villeneuve, N., Bachèlery, P., and Kemp, J.: La Réunion Island: A Typical Example of a Basaltic Shield Volcano with Rapid Evolution, in: Landscapes and Landforms of France, edited by Fort, M. and André, M.-F., pp. 261–270, Springer Netherlands, Dordrecht, https://doi.org/10.1007/978-94-007-7022-5_25, 2014.

Vittecoq, B., Reninger, P. A., Violette, S., Martelet, G., Dewandel, B., and Audru, J. C.: Heterogeneity of Hydrodynamic Properties and Groundwater Circulation of a Coastal Andesitic Volcanic Aquifer Controlled by Tectonic Induced Faults and Rock Fracturing – Martinique Island (Lesser Antilles – FWI), Journal of Hydrology, 529, 1041–1059, https://doi.org/10.1016/j.jhydrol.2015.09.022, 2015.

Vittecoq, B., Reninger, P.-A., Lacquement, F., Martelet, G., and Violette, S.: Hydrogeological Conceptual Model of Andesitic Watersheds Revealed by High-Resolution Heliborne Geophysics, Hydrology and Earth System Sciences, 23, 2321–2338, https://doi.org/10.5194/hess-23-2321-2019, 2019.

Voight, B.: Structural Stability of Andesite Volcanoes and Lava Domes, Philosophical Transactions of the Royal Society of London. Series A: Mathematical, Physical and Engineering Sciences, 358, 1663–1703, https://doi.org/10.1098/rsta.2000.0609, 2000.

Voight, B., Janda, R. J., Glicken, H., and Douglass, P. M.: Nature and Mechanics of the Mount St Helens Rockslide-Avalanche of 18 May 1980, Géotechnique, 33, 243–273, https://doi.org/10.1680/geot.1983.33.3.243, 1983.

Wan, C. F. and Fell, R.: Assessing the Potential of Internal Instability and Suffusion in Embankment Dams and Their Foundations, Journal of Geotechnical and Geoenvironmental Engineering, 134, 401–407, https://doi.org/10.1061/(ASCE)1090-0241(2008)134:3(401), 2008.

Westercamp, D., Andreieff, P., Bouysse, P., Cottez, S., and Battistini, R.: Carte Géologique France, Feuille Martinique, 1989.